

# Sparse Structures for Multivariate Extremes

Sebastian Engelke<sup>1</sup> and Jevgenijs Ivanovs<sup>2</sup>

<sup>1</sup>Research Center for Statistics, University of Geneva, Boulevard du Pont d'Arve 40, 1205 Geneva, Switzerland; email: sebastian.engelke@unige.ch

<sup>2</sup>Department of Mathematics, Aarhus University, Ny Munkegade 118, 8000 Aarhus, Denmark; email: jevgenijs.ivanovs@math.au.dk

Xxxx. Xxx. Xxx. Xxx. YYYY. AA:1–32

[https://doi.org/10.1146/\(\(please add article doi\)\)](https://doi.org/10.1146/((please add article doi)))

Copyright © YYYY by Annual Reviews.  
All rights reserved

## Keywords

Extreme value theory, conditional independence, dimension reduction, extremal graphical models, sparsity

## Abstract

Extreme value statistics provides accurate estimates for the small occurrence probabilities of rare events. While theory and statistical tools for univariate extremes are well-developed, methods for high-dimensional and complex data sets are still scarce. Appropriate notions of sparsity and connections to other fields such as machine learning, graphical models and high-dimensional statistics have only recently been established. This article reviews the new domain of research concerned with the detection and modeling of sparse patterns in rare events. We first describe the different forms of extremal dependence that can arise between the largest observations of a multivariate random vector. We then discuss the current research topics including clustering, principal component analysis and graphical modeling for extremes. Identification of groups of variables which can be concomitantly extreme is also addressed. The methods are illustrated with an application to flood risk assessment.

## Contents

1. Introduction .....	2
1.1. Overview .....	3
1.2. Application to flood risk assessment in Switzerland .....	4
2. Preliminaries .....	4
2.1. Recap of univariate theory .....	4
2.2. Extremal dependence coefficients .....	6
2.3. Multivariate regular variation .....	6
2.4. Properties of the exponent measure .....	8
2.5. Empirical estimation .....	9
3. Classical models and their limitations .....	10
4. Adaptation of unsupervised learning methods .....	12
4.1. Clustering approaches .....	12
4.2. Principal component analysis .....	13
4.3. Application to flood risk .....	14
5. Concomitant extremes .....	14
5.1. Detecting faces with $\Lambda$ -mass .....	16
5.2. Detecting maximal faces with $\Lambda$ -mass .....	17
5.3. Application to flood risk .....	18
6. Graphical models for extremes .....	19
6.1. Max-stable distributions .....	21
6.2. Multivariate Pareto distributions .....	22
6.3. Application to flood risk .....	25

## 1. Introduction

Flooding, heat waves and high concentrations of pollutants in the air are examples of environmental risks that are driven by very few rare events. Such events can have devastating impact on human life and can cause huge physical damage. Recent financial crises have likewise shown how underestimating the tails of loss distributions can underestimate systemic economic risks. The accurate statistical assessment of the small probabilities of occurrence of such extreme scenarios is thus crucial in many different settings. Extreme value theory is a widely-used approach to quantify the risk of these rare events. It provides mathematically justified tools to extrapolate beyond the data range and to estimate return periods of events that have never yet been observed.

In complex systems, such as rivers or financial networks, the most catastrophic events are due to concatenations of several rare events. Inundation of a lower river basin is typically the result of cumulation of simultaneous river exceedances in the upper river basin (e.g., Keef et al. 2009, Asadi et al. 2015). In climate science, extreme impacts such as fires or droughts are driven by joint extremes of several meteorological variables (e.g., Westra & Sisson 2011, Zscheischler & Seneviratne 2017, Engelke et al. 2019a). Similarly, the systemic risk of a financial system highly depends on the connections among core institutions (e.g., Poon et al. 2004, Zhou 2010, McNeil et al. 2015). In all these applications, the multivariate dependence between univariate rare events will determine the severity of risk for the whole system. Multivariate extreme value statistics therefore concentrates on dependence modeling in complex multivariate or spatial systems (cf., Davison et al. 2012). While research is very

active in this area, most applications are still limited to fairly moderate dimensions due to a lack of clear notions of sparsity in this context.

This review describes the existing literature, recent advances and future directions in the mathematical theory and statistical methodology for modeling dependence and detecting sparse patterns for extremes in higher dimensions.

### 1.1. Overview

The definition of extreme values implies that only few observations in a data set contain an informative signal on the distributional tail. Research on multivariate extremes in the last decades has thus concentrated on parsimonious modeling in cases where domain knowledge is available. A major branch with many applications in meteorology is the analysis of spatial extreme events, where information on the geographical locations of measurement stations significantly simplifies extremal dependence modeling. In many applications, however, such knowledge is insufficient or even unavailable, as for instance in risk analysis of financial networks where connections between the institutions are unknown. Especially in higher dimensions and complex situations it therefore becomes essential to exploit underlying structures and to learn sparse patterns in a data driven way.

Dependence between extreme observations of a random vector  $X = (X_1, \dots, X_d)$  can exhibit complicated structures (cf., Ledford & Tawn 1997, Coles et al. 1999) and the notions of sparsity, conditional independence and dimension reduction are sometimes different from the non-extreme world. Many recent works in extreme value statistics have started to establish links to other fields such as graphical models, machine learning and causality, and to adapt classical methods for the detection of sparse structures in multivariate data. The different approaches can be grouped into three broad areas of research.

- (i) The first class of approaches concentrates on methods from unsupervised learning such as clustering and principal component analysis, and adapts them to the context of extreme observations. These non-parametric dimension reduction techniques are mostly used for exploratory analysis and visualization of extremal dependence (cf., Chautru 2015, Cooley & Thibaud 2019, Drees & Sabourin 2019, Janssen & Wan 2019).
- (ii) The second notion of sparsity is inherent to rare event analysis. It relates to the study of concomitant extremes, that is, which sub-groups of variables in the multivariate random vector  $(X_1, \dots, X_d)$  are likely to take large values simultaneously. Sparse models should only exhibit a small number of such groups and their detection is a challenging task. Statistically this is related to estimating the support of a measure on a  $d$ -dimensional space and several inferential methods have been proposed (cf., Goix et al. 2017, Chiapino & Sabourin 2017, Chiapino et al. 2019, Meyer & Wintenberger 2019, Simpson et al. 2018).
- (iii) One classical way to define probabilistic sparsity is through conditional independence structures and graphical models, since they allow the decomposition of high-dimensional distributions into low-dimensional components. Graphical models in extreme value statistics have only recently been introduced and studied (cf., Gissibl & Klüppelberg 2018, Engelke & Hitz 2019, Segers 2019). These developments open new fields of research at the interface of extremes, structure learning, high-dimensional inference and causality (cf., Mhalla et al. 2019, Gnecco et al. 2019, Engelke & Volgushev 2020).

This review begins with a background on the fundamental objects of multivariate extreme value theory in Section 2. The classical statistical modeling strategies and their limitations are briefly described in Section 3. Sections 4, 5 and 6 discuss the three main research directions for sparsity detection outlined above. Each time, a clear definition of the sparsity notion used in the respective section is given.

Our review conveys the main ideas in sparse modeling of extremes, but the literature is vast and our references are necessarily selective. Further interesting topics that are beyond the scope of this article include the modeling of asymptotically independent extremes (e.g., Heffernan & Tawn 2004, Wadsworth & Tawn 2012, Papastathopoulos et al. 2017), flexible models between different dependence classes (e.g., Wadsworth et al. 2017, Huser & Wadsworth 2019, Engelke et al. 2019c) and connections of extreme values to the theory of networks (e.g., Samorodnitsky et al. 2016, Wan et al. 2020).

## 1.2. Application to flood risk assessment in Switzerland

We illustrate the different methods of this review on sparse structures for extremes using river discharges at  $d = 68$  locations in Switzerland, mostly in the Rhine and Aare catchments. Figure 1 shows the basin with its topography and the gauging stations. The data are monitored by the Swiss Federal Office of the Environment and consist of daily average discharges. The length of the recorded time series at the 68 locations is between 30 and 120 years. For simplicity we only use the summer months June, July and August, and only data with records for all locations. This results in 22 years of common summer discharges, that is,  $n = 2024$  daily observations.

Accurate quantification of the risk related to large peak river flows is crucial for effective flood protection. A univariate extreme value analysis of the tails at each of the 68 stations has been done in Asadi et al. (2018). Analyzing the extremal dependence structure of river discharges requires a wide range of statistical tools. This includes the identification of groups of locations where floods may happen simultaneously, the statistical modeling of these concomitant extremes and the simulation of multivariate rare events for worst case analyses.

River networks are highly complex systems and the dependence between extremes at different locations can not be sufficiently explained by spatial Euclidean distances as it is common in geostatistical applications for precipitation, for instance. In addition to this, the largest discharges may be dampened by big lakes or affected by hydroelectric installations. For this data set on river flows it is thus highly relevant to understand the extremal dependence and we expect sparse patterns and an underlying, non-trivial probabilistic structure.

## 2. Preliminaries

### 2.1. Recap of univariate theory

Univariate extreme value theory is a well-established topic and many statistical tools exist to analyze the tail of a random variable  $X$ . In the most basic setting, given independent observations  $X^{(1)}, \dots, X^{(n)}$  of  $X$ , we are interested in estimating the survival function  $1 - F(t) = \mathbb{P}(X > t)$  for large  $t$ . Here ‘large’ is understood as being close to the maximal possible value  $t_\infty = \sup\{t : F(t) < 1\}$ , known as the upper endpoint of  $F$ .

There are two main modeling strategies based on different limiting probability models: the block maxima method and the peaks-over-threshold approach. For the former, we

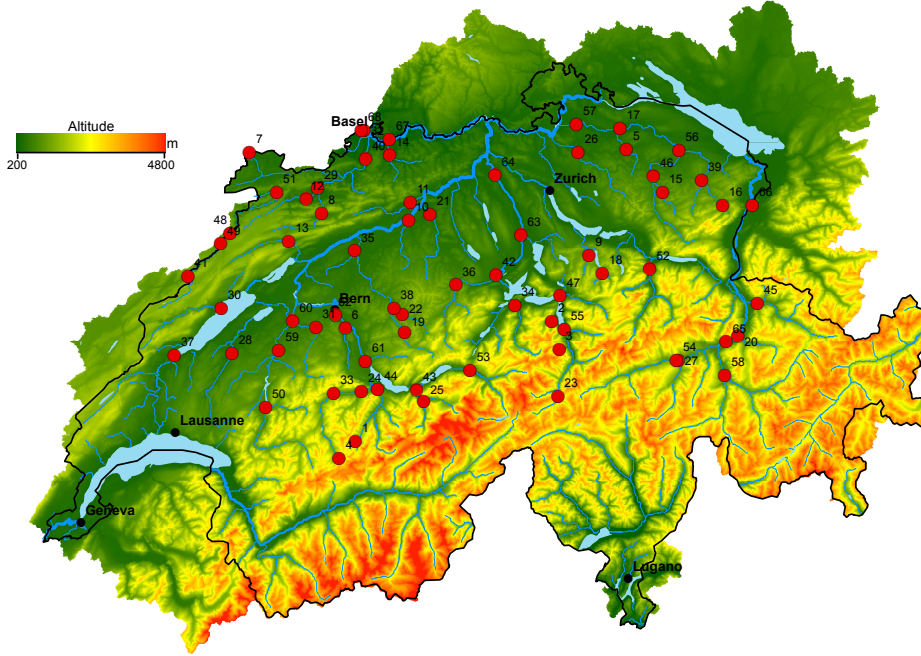


Figure 1: Topographic map of Switzerland showing sites of 68 gauging stations (red dots) mostly along the Rhine, the Aare and their tributaries.

assume that the sequence of normalized maxima converges in distribution to some non-degenerate limit,

$$\frac{\max(X_1, \dots, X_n) - b_n}{a_n} \xrightarrow{d} Z, \quad n \rightarrow \infty, \quad 1.$$

for some  $a_n > 0, b_n \in \mathbb{R}$ . The distribution of  $Z$  belongs to the class of generalized extreme value distributions (Fisher & Tippett 1928), which is parameterized by its shape, location and scale parameters. Such  $Z$  is also called max-stable because the maximum of independent copies of  $Z$  can be affinely normalized to get back the distribution of  $Z$ . The convergence in Equation 1 is equivalent to the convergence of scaled exceedances to a non-degenerate limit (Balkema & de Haan 1974),

$$\frac{X - t}{c_t} \Big| \{X > t\} \xrightarrow{d} Y, \quad t \rightarrow t_\infty, \quad 2.$$

for some  $c_t > 0$ , which underlies the peaks-over-threshold approach. The limit  $Y$  has a generalized Pareto distribution (Pickands 1975), parameterized by a shape and a location parameter. Importantly,  $Z$  and  $Y$  are closely related and they share the same shape parameter.

For a detailed overview of univariate extreme value theory and a further references we refer to the textbooks Embrechts et al. (1997), Coles (2001), Beirlant et al. (2004), de Haan & Ferreira (2006) and Resnick (2008), and to the review articles Katz et al. (2002) and Davison & Huser (2015).

## 2.2. Extremal dependence coefficients

Consider a  $d$ -dimensional random vector  $X = (X_j : j \in V)$ , where here and in the sequel  $V = \{1, \dots, d\}$  denotes the index set. Our interest is in the probability that some (or all) components of  $X$  are large. This probability is strongly influenced by the dependence between the extreme observations of the  $d$  single variables. Extremal dependence may take many different forms. For two components  $X_i$  and  $X_j$ , a first broad split can be done through the (upper) tail dependence coefficient, which is defined as

$$\chi_{ij} = \lim_{q \rightarrow 1} \chi_{ij}(q) = \lim_{q \rightarrow 1} \mathbb{P}(F_i(X_i) > q, F_j(X_j) > q) / (1 - q) \in [0, 1], \quad 3.$$

whenever the limit exists and where  $F_i$  is the distribution function of  $X_i$ . It quantifies the conditional probability that both components are large given that one is large. If the coefficient  $\chi_{ij} > 0$ , the variables  $X_i$  and  $X_j$  are said to exhibit asymptotic dependence. In the case  $\chi_{ij} = 0$  we have asymptotic independence, and then one often assumes that

$$\mathbb{P}(F_i(X_i) > q, F_j(X_j) > q) = (1 - q)^{1/\eta_{ij}} \ell(1 - q), \quad \eta_{ij} \in [0, 1], \quad 4.$$

where the function  $\ell : [0, 1] \rightarrow \mathbb{R}_+$  is slowly varying at zero. The coefficient  $\eta_{ij}$  is called residual tail dependence coefficient and has been introduced by Ledford & Tawn (1997) and studied in Peng (1999), Ramos & Ledford (2009), de Haan & Zhou (2011) and Eastoe & Tawn (2012). It describes the rate of convergence of the joint exceedance probability to zero, and in the case of asymptotic dependence we have  $\eta_{ij} = 1$ . For most bivariate distributions the coefficients  $\chi_{ij}$  and  $\eta_{ij}$  can be computed explicitly (e.g., Engelke et al. 2019c).

We may extend the definition of both tail dependence coefficients in Equations 3 and 4 to any non-empty subset  $I \subset V = \{1, \dots, d\}$  by considering joint exceedances of the components  $X_i$ ,  $i \in I$ , and we denote them by  $\chi_I$  and  $\eta_I$ . The set of coefficients  $\chi_I$  and  $\eta_I$  for all non-empty  $I \subsetneq V$  must satisfy the consistency constraint

$$\sum_{J \supset I} (-1)^{|J \setminus I|} \chi_J \geq 0, \quad \forall J \supset I \quad \eta_J \leq \eta_I. \quad 5.$$

Conversely, any such vectors  $(\chi_I)$  and  $(\eta_I)$  with elements in  $[0, 1]$  and  $\chi_I > 0$  implying  $\eta_I = 1$  can arise as tail dependence coefficients for some  $d$ -dimensional vector  $X$ . Equation 5 further implies the monotonicity  $\chi_J \leq \chi_I$  for all  $J \supset I$ . The above consistency result essentially follows from de Haan & Zhou (2011); see also Schlather & Tawn (2002) and Stokorb & Schlather (2015) for some further theory.

The coefficients presented here are summaries of the extremal dependence of the vector  $X$ . For a multivariate data set, a first exploratory analysis includes plots of empirical estimates of the bivariate coefficients  $\hat{\chi}_{ij}(q)$  for a range of threshold levels  $q$  close to one. This helps to distinguish between the regimes of asymptotic dependence and independence and guides later modeling choices. For the Swiss river data from Section 1.2, Figure 2 shows such plots for two pairs of stations. The curve in left-hand side plot corresponding to two close-by stations is stable around a positive level, indicating asymptotic dependence. The curve in the right-hand side plot corresponds to two stations far apart, and it tends to zero for  $q \rightarrow 1$ , which suggests asymptotic independence.

## 2.3. Multivariate regular variation

In multivariate extremes the problem of analyzing the tail of the vector  $X$  is usually divided into two steps, modeling of marginal tails and modeling of the extremal dependence. While

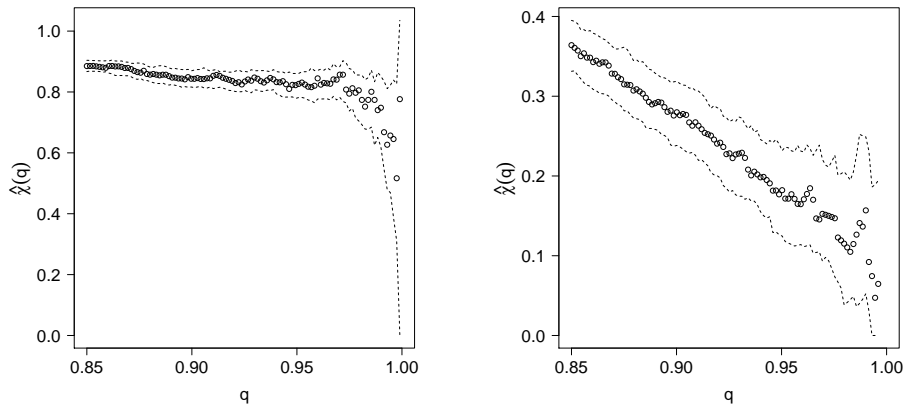


Figure 2: Empirical estimates  $\hat{\chi}_{ij}(q)$  of the tail dependence coefficient for a range of thresholds  $q$  for  $i = 56$  and  $j = 57$  (left), and  $i = 1$  and  $j = 56$  (right). Dashed lines are 95% bootstrap confidence intervals.

the former step is described in Section 2.1, for the latter we standardize the marginals to focus exclusively on extremal dependence. The common choice is the standard Pareto distribution and we assume in sequel that  $\mathbb{P}(X_j \leq x) = 1 - 1/x$  for  $x \geq 1$  and  $j \in V$ . For a continuous marginal distribution  $F_j$  this amounts to a simple transformation  $1/\{1 - F_j(X_j)\}$ . This procedure brings all the components to the same scale, so that ‘large’ is now understood in the same way. In practice, this transformation can be done empirically (cf., Section 2.5), or based on a parametric or semi-parametric estimate of  $F_j$ .

Similarly to the univariate setting, in multivariate extreme value theory there exist two intimately linked methods to study the tail of the random vector  $X$ , namely the maxima approach and the peaks-over-threshold approach. For the former, we consider component-wise maxima  $M_n = \max(X^{(1)}, \dots, X^{(n)})$  of independent copies of the random vector  $X$ , that is, the  $j$ th component is  $M_{nj} = \max_{i=1, \dots, n} X_j^{(i)}$ . We assume that  $M_n$  weakly converges as  $n \rightarrow \infty$ , when properly normalized, to some random vector  $Z$ ; see also Equation 1 for the univariate case. Since  $X$  has standard Pareto margins, the normalization simplifies and we have  $M_n/n \xrightarrow{d} Z$ , and the marginals of  $Z$  are standard Fréchet. The random vector  $Z$  is called max-stable and its distribution can be represented as

$$\mathbb{P}(Z \leq z) = \exp\{-\Lambda_z\} = \exp\{-\Lambda(\mathcal{E} \setminus [0, z])\}, \quad z \geq 0, \quad 6.$$

where the so-called exponent measure  $\Lambda$  defined on the space  $\mathcal{E} = [0, \infty)^d \setminus \{0\}$  satisfies  $\Lambda(A) < \infty$  for all Borel sets  $A \subset \mathcal{E}$  bounded away from the origin. A standard argument shows that the above convergence of normalized maxima is equivalent to

$$\lim_{t \rightarrow \infty} t\mathbb{P}(X/t \in A) = \Lambda(A), \quad 7.$$

for all  $\Lambda$ -continuous Borel sets  $A \subset \mathcal{E}$  bounded away from the origin. The regularity assumption in Equation 7 is called multivariate regular variation. Importantly, it suggests a simple way of extrapolating the probability law from, say, moderately large values into tail regions having few or no observations.

While under multivariate regular variation the componentwise maxima converge to the max-stable  $Z$  defined in Equation 6, the exceedances over a high threshold converge to a multivariate Pareto distribution  $Y$  (cf., Rootzén & Tajvidi 2006),

$$\mathbb{P}(Y \leq z) = \lim_{t \rightarrow \infty} \mathbb{P}(X/t \leq z \mid \|X\|_\infty > t) = \frac{\Lambda_{\min(z,1)} - \Lambda_z}{\Lambda_1}, \quad z \in \mathcal{L}, \quad 8.$$

where the support  $\mathcal{L} = \{x \in \mathcal{E} : \|x\|_\infty \geq 1\}$  is the positive orthant with the unit cube removed. This approximation follows from Equation 7 and it also implies that the law of  $Y$  is proportional to  $\Lambda$  restricted to  $\mathcal{L}$ .

Throughout the paper we assume that  $X$  is multivariate regularly varying as defined in Equation 7.

## 2.4. Properties of the exponent measure

The exponent measure  $\Lambda$  contains all information on the extremal dependence of  $X$ . Equation 7 immediately implies that it is homogeneous of order  $-1$ , that is,  $\Lambda(cA) = c^{-1}\Lambda(A)$  for  $c > 0$ . It is often convenient to switch to polar coordinates, and thus we consider some norm  $\|\cdot\|$ ; the usual choices are the  $\ell_1$ -norm  $\|z\|_1 = \sum_i |z_i|$  and  $\ell_\infty$ -norm  $\|z\|_\infty = \max_i |z_i|$ . Define the positive simplex  $\mathbb{S}_+^{d-1} = \{z \in \mathcal{E} : \|z\| = 1\}$ , so that each  $z \in \mathcal{E}$  can be written as  $z = \|z\|\theta$ , where  $\theta = z/\|z\| \in \mathbb{S}_+^{d-1}$  is the corresponding angle. Homogeneity implies that  $\Lambda$  decomposes into an angular part and an independent radial part

$$\Lambda\{z \in \mathcal{E} : \|z\| \geq r, z/\|z\| \in \cdot\} = cr^{-1}\mathbb{P}(\Theta \in \cdot), \quad \forall r > 0, \quad 9.$$

where  $c = \Lambda\{z \in \mathcal{E} : \|z\| > 1\}$  is a fixed constant and  $\Theta$  follows the so-called angular (or spectral) distribution  $H$  on  $\mathbb{S}_+^{d-1}$ . From Equation 7 we also have

$$\lim_{t \rightarrow \infty} \mathbb{P}\left(\frac{X}{\|X\|} \in \cdot \mid \|X\| > t\right) = \mathbb{P}(\Theta \in \cdot), \quad 10.$$

leading to the interpretation of  $\Theta$  as the limiting extremal angle for high threshold exceedances. For a textbook treatment of multivariate regular variation we refer to Resnick (2008), and to Basrak et al. (2002) and Lindskog et al. (2014) for further theory.

Under multivariate regular variation all tail dependence coefficient in Equation 3 exist and  $\chi_I = \Lambda(x_i > 1 \forall i \in I)$ . Groups of components  $(X_i : i \in I)$  that can be large simultaneously correspond to the non-empty subsets  $I \subset V$  with  $\chi_I > 0$ . We can partition  $\mathcal{E}$  into  $2^d - 1$  disjoint sub-cones, the faces of all dimensions,

$$\mathcal{E}_I = \{x \in \mathcal{E} : x_i > 0 \forall i \in I, x_j = 0 \forall j \notin I\}, \quad 11.$$

and we note that  $\Lambda(\mathcal{E}_I) > 0$  indicates that the components  $(X_i : i \in I)$  can be extreme while the components  $(X_i : i \notin I)$  are much smaller. Equivalently, this can be formulated in terms of the multivariate Pareto  $Y$  or the angular measure  $H$ . In particular, mass of  $\Lambda$  in  $\mathcal{E}_V$ , the interior of  $\mathcal{E}$ , means that all components can be extreme at the same time. In principle, almost any collection of faces may have  $\Lambda$ -mass, resulting in order of  $2^{2^d}$  possible combinations. Thus the extremal dependence between the components of  $X$  may have a complicated structure with both asymptotic dependence and independence present. In dimension  $d = 3$ , Figure 3 shows the  $\ell_1$ -simplex  $\mathbb{S}_+^2$  and its intersections with the 7 different faces  $\mathcal{E}_I$ , together with the observations of the extremal angle  $\Theta$  for three stations of the river data set from Section 1.2.



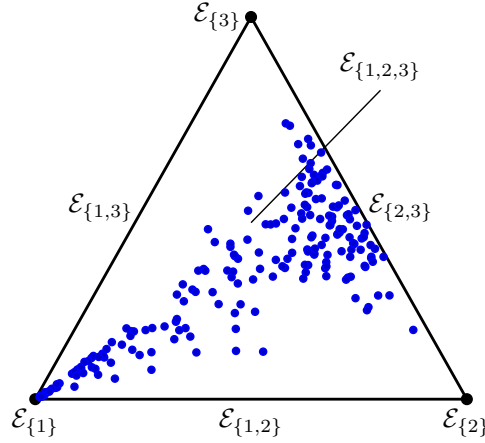


Figure 3: The simplex  $\mathbb{S}_+^2$  with empirical extremal angles corresponding to the sub-group  $\{1, 56, 57\}$  of stations.

If the exponent measure  $\Lambda$  is absolutely continuous with respect to  $d$ -dimensional Lebesgue measure we denote its density by  $\lambda$ . In this case, both the max-stable distribution  $Z$  and the multivariate Pareto distribution  $Y$  also possess densities. More generally,  $Z$  has a density if and only if  $\Lambda$  has a density on each face  $\mathcal{E}_I$ ,  $I \subset V$  (Dombry et al. 2017a).

## 2.5. Empirical estimation

The exponent measure  $\Lambda$  can be estimated empirically. Let  $X^{(1)}, \dots, X^{(n)}$  be independent observations of the random vector  $X$ . Using Equation 7 with  $t = n/k$ , we define an empirical estimator of  $\Lambda_z = \Lambda(\mathcal{E} \setminus [0, z])$ ,  $z \in \mathcal{E}$ , by

$$\hat{\Lambda}_z = \frac{1}{k} \sum_{i=1}^n \mathbf{1} \left\{ \hat{F}_1(X_1^{(i)}) > 1 - \frac{k}{nz_1} \text{ or } \dots \text{ or } \hat{F}_d(X_d^{(i)}) > 1 - \frac{k}{nz_d} \right\}, \quad 12.$$

where  $k = k(n)$  can be interpreted as the number of exceedances. Here, the application of the empirical distribution function  $\hat{F}_j$  corresponds to the standardization explained in Section 2.3. This estimator is closely related to the empirical estimator of stable tail dependence function, whose asymptotic behavior is well studied (cf., de Haan & Ferreira 2006). Under the standard assumption that  $k \rightarrow \infty$  and  $k/n \rightarrow 0$ ,  $\hat{\Lambda}_z$  is a consistent estimator of  $\Lambda_z$ , and under appropriate second-order conditions it is asymptotically normal even in a functional sense as a process indexed by  $z \in \mathcal{E}$  (cf., Huang 1992, Drees & Huang 1998, Einmahl et al. 2012a, Bücher et al. 2014). The estimators in Figure 2 are obtained as  $\hat{\chi}_{ij}(q) = 2 - \hat{\Lambda}_{(1,1)}$  with  $q = 1 - k/n$  for a range of values for  $k$ .

Using a similar counting approach as in Equation 12, we can define the empirical version  $\hat{H}$  of the angular distribution  $H$  of the extremal angles  $\Theta$  based on Equation 10, and asymptotic theory for this estimator can be derived.

### 3. Classical models and their limitations

In the last decades, there has been active research on the construction of statistical models for multivariate extremes. In this section we give a brief overview of the literature and mention some of the models that appear in later parts of the review. We also describe the limitations of these classical approaches when facing more complex data sets in higher dimensions. One of the simplest models is the max-linear model.

**Example 1** (Max-linear model). *Let  $\varepsilon_i$ ,  $i = 1, \dots, p$  be independent standard Fréchet variables and  $A = (a_{ij})$  be a  $d \times p$  matrix of non-negative coefficients. Define a  $d$ -dimensional random vector  $Z$  with entries*

$$Z_i = \max(a_{i1}\varepsilon_1, \dots, a_{ip}\varepsilon_p), \quad i = 1, \dots, d. \quad 13.$$

*We assume that the rows of  $A$  sum up to 1, ensuring that all  $Z_i$  have standard Fréchet distributions. The max-linear model is max-stable with exponent measure  $\Lambda$  supported on  $p$  rays specified by the columns of  $A$ , or in other words, the angle  $\Theta$  takes  $p$  possible values  $a_{\cdot j}/\|a_{\cdot j}\|$  with probabilities proportional to  $\|a_{\cdot j}\|$ .*

Every max-stable distribution whose angular measure  $H$  concentrates on finitely many points corresponds to a max-linear model; see Yuen & Stoev (2014) for details. For applications, max-linear models are often too simplistic but they may provide a first approximation of the data and are useful tools to illustrate statistical methods. For instance, it is easy to construct a max-linear model whose exponent measure has support on any combination of faces of  $\mathcal{E}$ . More realistic parametric model classes are often specified in terms of the exponent measure density  $\lambda$ .

**Example 2** (Logistic distribution). *The  $d$ -dimensional extremal logistic distribution with parameter  $\theta \in (0, 1)$  has exponent measure density*

$$\lambda(y) = \left( \sum_{i=1}^d y_i^{-1/\theta} \right)^{\theta-d} \prod_{i=1}^{d-1} \left( \frac{i}{\theta} - 1 \right) \prod_{i=1}^d y_i^{-1/\theta-1}, \quad y \in \mathcal{E}. \quad 14.$$

*The strength of dependence between all components ranges from complete dependence for  $\theta \rightarrow 0$  to independence for  $\theta \rightarrow 1$ .*

The logistic distribution is symmetric and has only one parameter  $\theta$ , independently of the dimension. The asymmetric logistic distribution (Tawn 1988) is an extension that is more flexible, but at the price of an order of  $2^d$  parameters in dimension  $d$ . A parametric family with good control of extremal dependence between any pair of components is the distribution introduced in Hüsler & Reiss (1989). For this, and many other reasons, it can be seen as the Gaussian distribution for asymptotically dependent extremes.

**Example 3** (Hüsler–Reiss distribution). *This distribution is parameterized by a variogram matrix  $\Gamma = (\Gamma_{ij})_{i,j \in V}$  and its exponent measure density can be written for any  $m \in V$  as (cf., Engelke et al. 2015)*

$$\lambda(y) = y_m^{-2} \prod_{i \neq m} y_i^{-1} \phi_{d-1} \left( \log(y_{-m}/y_m) + \Gamma_{-m,m}/2; \Sigma^{(m)} \right), \quad y \in \mathcal{E}, \quad 15.$$

where  $\phi_p(\cdot; \Sigma)$  is the density of a centered  $p$ -dimensional normal distribution with covariance matrix  $\Sigma$ , the notation  $-m$  in a vector or matrix means omission of the index  $m$ , and

$$\Sigma^{(m)} = \frac{1}{2} \{\Gamma_{im} + \Gamma_{jm} - \Gamma_{ij}\}_{i,j \in V \setminus \{m\}} \in \mathbb{R}^{(d-1) \times (d-1)}. \quad 16.$$

The strength of dependence between the  $i$ th and  $j$ th components is parameterized by  $\Gamma_{ij}$ , ranging from complete dependence for  $\Gamma_{ij} = 0$  and independence for  $\Gamma_{ij} = \infty$ .

There are many further multivariate models such as the Dirichlet mixture model in Boldi & Davison (2007) or the pairwise beta distribution in Cooley et al. (2010); we refer to Gudendorf & Segers (2010) for a detailed overview.

All of these model classes become restrictive in higher dimensions, either because of a lack of flexibility or a rapid increase in the number of parameters. Parsimonious extreme value models in large dimensions have been developed for spatial applications, where the vector  $X$  is recorded at  $d$  locations  $t_1, \dots, t_d \in \mathbb{R}^D$  in space. Following ideas from geostatistics (cf., Wackernagel 2013), extremal dependence is then parameterized in terms of distances  $\|t_i - t_j\|$ , which drastically reduces the number of required parameters. Brown–Resnick processes (Brown & Resnick 1977, Kabluchko et al. 2009) for instance, are the extension of Hüsler–Reiss distributions to random fields and they are widely used models for spatial rare events. Other models for such max-stable processes have been introduced in Schlather (2002), Opitz (2013) and Reich & Shaby (2012), in Davis et al. (2013) and Davison & Huser (2015) for the spatio-temporal setting, and in Asadi et al. (2015) for river networks. Without domain knowledge such as the spatial locations of gauging stations, these models can no longer be applied. For general multivariate data, there are some approaches to define low-dimensional parametric representations through copulas (Aas et al. 2009, Lee & Joe 2018), graphical constructions (Hitz & Evans 2016) and elliptical distributions (Haug et al. 2009), or as ensembles of trees (Yu et al. 2017).

Statistical inference for multivariate extreme value models is challenging, and the related literature is vast. Maximum likelihood estimation is commonly used (e.g., Engelke et al. 2015, Wadsworth & Tawn 2014, Thibaud et al. 2016) but can be computationally demanding due to censoring that is applied to non-extreme components (cf., Ledford & Tawn 1997). Alternative methods include pairwise likelihood (e.g., Varin et al. 2011, Padoan et al. 2010),  $M$ -estimation (e.g., Einmahl et al. 2012b, 2016) and proper scoring rules (de Fondeville & Davison 2018). Exact simulation of these models, both conditional and unconditional, has also been studied (Dombry et al. 2013, Dieker & Mikosch 2015, Dombry et al. 2016).

While spatial models have few parameters even in high dimensions, they possess some major limitations. On the one hand, they require prior domain knowledge on the spatial locations of gauging stations and rely on the strong assumption of stationarity in space. It is not possible to learn the underlying structure from the data. On the other hand, even though these models have few parameters, their distributions do generally not exhibit any sparsity properties in a probabilistic sense, such as conditional independence patterns or support on low-dimensional sub-spaces. This means that statistical inference does not simplify and likelihood inference is limited to fairly moderate dimensions (Thibaud et al. 2016, Dombry et al. 2017b, Huser et al. 2019).

In the next sections we present a new line of research providing alternatives to these classical methods. They learn sparse structures and low-dimensional representations in multivariate extreme values in a data driven way and do not require additional domain knowledge or stationarity assumptions.

## 4. Adaptation of unsupervised learning methods

Clustering and principal component analysis are two of the standard methods in multivariate analysis (cf., Anderson 2003). They are both tools to detect lower-dimensional representations of the data. For extremes, there is recent work that adapts these tools to find structures in multivariate tails assuming the following notion of sparsity.

(S1) The dimension of the support of the exponent measure  $\Lambda$  is much smaller than  $d$ .

In other words, the exponent measure can be expressed via a low-dimensional object. In this section we describe the expanding literature in this field.

### 4.1. Clustering approaches

Centroid-based clustering aims at finding the set of  $p$  points  $c_1, \dots, c_p \in \mathbb{R}^d$ , called cluster centers, that minimize the cost

$$\mathbb{E} \min_{j=1}^p \varrho(\Theta, c_j), \quad 17.$$

where  $\Theta \in \mathbb{R}^d$  is a random object of interest and  $\varrho$  is a given distance or dissimilarity function. In the setting of extremes the main focus is on the case where  $\Theta$  is the extremal angle with distribution  $H$  appearing in the decomposition of the exponent measure  $\Lambda$  in Equation 9. The above optimization problem is computationally hard and usually heuristic algorithms are used that exhibit fast convergence to a local optimum. Clustering is mainly an exploratory tool which may lead to dimension reduction in two ways. Firstly, the associated cost may become small for a moderate number of clusters  $p$ . This happens when the angular distribution concentrates at a small number of points in  $\mathbb{S}_+^{d-1}$ , thereby hinting at a max-linear model as in Example 1 and a sparse representation as in (S1). Secondly, all of the cluster centers may have multiple small entries indicating that  $H$  puts mass only on some faces of  $\mathbb{S}_+^{d-1}$ ; see Section 5 for this notion of sparsity.

Chautru (2015) and Janssen & Wan (2019) propose clustering the angle  $\Theta$  using the spherical  $k$ -means procedure of Dhillon & Modha (2001), which ensures that cluster centers also belong to the simplex  $\mathbb{S}_+^{d-1}$ . Janssen & Wan (2019) employ the angular dissimilarity

$$\varrho(x, y) = 1 - \cos(x, y) = 1 - \frac{x^\top y}{\|x\|_2 \|y\|_2}, \quad 18.$$

which is independent of the norm used to define  $\Theta$ . They establish a consistency result showing that cluster centers obtained from the empirical distribution of angles  $\hat{H}$  (cf., Section 2.5) converge to the cluster centers of the true angular distribution  $H$ . It is noted, that this empirical approximation does depend on the choice of norm. They further investigate an application of this clustering method to inference for max-linear models defined in Equation 13, where the angular distribution  $H$  concentrates on  $p$  points  $a_{\cdot j} / \|a_{\cdot j}\| \in \mathbb{S}_+^{d-1}$ ,  $j = 1, \dots, p$ . This method provides estimates of the parameter vectors  $a_{\cdot j}$  that are competitive or even superior to other estimation methods considered by Yuen & Stoev (2014) and Einmahl et al. (2016, 2018). Finally, Janssen & Wan (2019) suggest using the cluster centers as ‘prototypes of directions of extremal events’, an idea that we adopt in our flood application in Section 5.3.

Clustering in the context of extremes is also considered in Bernard et al. (2013), however of a very different nature. They suggest grouping the components of  $X$  using a certain extremal dissimilarity similar to the pairwise tail dependence coefficients  $\chi_{ij}$  as the distance

between two components  $X_i$  and  $X_j$ ; see also Saunders et al. (2019) for an application of this method to rainfall extremes.

## 4.2. Principal component analysis

Principal component analysis (PCA) is a classical method of multivariate analysis to reduce the dimension of a random vector  $W \in \mathbb{R}^d$  while capturing most of its variability. PCA identifies the linear subspace  $\mathcal{S}^* \subset \mathbb{R}^d$  of a given dimension  $p < d$  so that the  $\ell_2$ -distance

$$\mathbb{E} \|\Pi_{\mathcal{S}^*} W - W\|_2^2 \quad 19.$$

between  $W$  and its projection  $\Pi_{\mathcal{S}^*} W$  onto  $\mathcal{S}^*$  is minimal (cf., Seber 1984), and thus  $\Pi_{\mathcal{S}^*} W$  can be seen as the best  $p$ -dimensional approximation of  $W$ . Fundamental to PCA are the orthonormal eigenvectors  $v_1, \dots, v_d \in \mathbb{R}^d$  of the positive semi-definite matrix  $\Sigma = \mathbb{E}(WW^\top)$ , ordered according to the respective eigenvalues  $\lambda_1 \geq \dots \geq \lambda_d \geq 0$ . The linear span of the first  $p$  eigenvectors  $v_1, \dots, v_p$  yields the desired  $\mathcal{S}^*$ , whereas the best  $p$ -dimensional approximation of  $W$  is obtained by summing up the respective orthogonal projections, called principal components,

$$\Pi_{\mathcal{S}^*} W = \Pi_{v_1} W + \dots + \Pi_{v_p} W.$$

Importantly, PCA results in an iterative procedure, often called reconstruction of  $W$ , where the principal components are added until the approximation error in Equation 19 drops below a certain threshold. For a zero mean vector  $W$  the optimization criterion in Equation 19 is equivalent to maximizing the variance of the projection  $\Pi_{\mathcal{S}^*} W$ . For statistical properties of PCA and theoretical guarantees we refer to Blanchard et al. (2007).

In the present setting one is interested, loosely speaking, in discovering a lower-dimensional linear subspace explaining most of the extreme behavior. Cooley & Thibaud (2019) and Drees & Sabourin (2019) consider the extremal angle  $\Theta$  with distribution  $H$  and the respective matrix

$$\Sigma = \mathbb{E}(\Theta\Theta^\top) = \lim_{t \rightarrow \infty} \mathbb{E} \left( \frac{XX^\top}{\|X\|^2} \mid \|X\| > t \right), \quad 20.$$

which has been introduced by Larsson & Resnick (2012) in the bivariate case. As explained above, the aim is to identify the optimal  $p$ -dimensional linear space  $\mathcal{S}^* \subset \mathbb{R}^d$  for  $\Theta$ . In applications, the distribution of  $\Theta$  is replaced by its empirical estimate  $\hat{H}$  (cf., Section 2.5). Drees & Sabourin (2019) show that, as the sample size  $n \rightarrow \infty$ , the corresponding optimal  $p$ -dimensional linear spaces converge in probability to the true  $\mathcal{S}^*$ , provided the latter is unique, with respect to the metric

$$\varrho(\mathcal{S}, \mathcal{S}') = \sup_{\theta \in \mathbb{S}_+^{d-1}} \|\Pi_{\mathcal{S}} \theta - \Pi_{\mathcal{S}'} \theta\|_2.$$

Importantly, the projection  $\Pi_{\mathcal{S}^*} \Theta$  does not necessarily belong to  $\mathbb{S}_+^{d-1}$ . Nevertheless, if the linear span of the support of  $H$  has dimension  $p$  then this linear span is the optimal  $\mathcal{S}^*$  and the loss in Equation 19 is zero. Intuitively, slight deviations from this assumption would lead to a projection in a neighborhood of  $\mathbb{S}_+^{d-1}$ , which then can be normalized/shifted appropriately. If the loss in Equation 19 is not negligible then this method may produce a sub-optimal approximation of  $\Theta$  in the given dimension  $p$ .

If the marginals of  $X$  are standardized so that the second moments exist, the above PCA for the angle  $\Theta$  is equivalent to PCA for the limit distribution of  $(X/t \mid \|X\| > t)$ , because the radial component becomes independent of the angle. Cooley & Thibaud (2019) follow this interpretation and suggest a way to reconstruct extreme scenarios of the original vector  $X$ . The problem that projections on  $\mathcal{S}^*$  may not belong to the domain of interest does however not disappear, and projections of  $X$  onto  $v_i$  may have negative entries. To remedy this, the authors propose projecting  $t^{-1}(X)$  on  $\mathcal{S}^*$  for some bijection  $t : \mathbb{R} \mapsto \mathbb{R}_+$  behaving as identity for large arguments, and then applying  $t$  to get back to the positive orthant. It is noted that the choice of the mapping  $t$  and the choice of the marginal distributions are somewhat arbitrary, but may have a major influence on the resulting approximation.

Chautru (2015) suggests using a technique called principal nested spheres developed by Jung et al. (2012). Firstly,  $\Theta$  is renormalized to lie on the  $\ell_2$ -sphere, and then it is projected on a sub-sphere of dimension  $d - 2$  formed by intersecting the original sphere with a hyperplane. Using numerical optimization, this sub-sphere is chosen to minimize the  $\ell_2$ -norm of the empirical geodesic distance to  $\Theta$ . The procedure is iterated until a certain loss exceeds a pre-defined threshold, thus resulting in a greedy search for a lower-dimensional approximation. In the setting of extreme angles, Chautru (2015) motivates the projection on sub-spheres by the problem of discovering mass of  $H$  on the faces; see also Section 5. Unlike PCA the final result may not be optimal and the computational effort is considerably larger. Furthermore, the approximation lies on the sphere but may not be in the positive orthant.

### 4.3. Application to flood risk

We conclude this section with an application to the river flow data set discussed in Section 1.2. As suggested by Drees & Sabourin (2019) and Cooley & Thibaud (2019) we apply PCA to the matrix  $\Sigma$  in Equation 20. We use the empirical 90%-quantile of the radius  $\|X\|$  as the threshold and compute the estimate  $\hat{\Sigma}$  based on the approximate extremal angles of the  $k = 202$  exceedances (cf., Section 2.5). We do not use temporal declustering since Zou et al. (2019) show that the use of a larger but possibly dependent data set can decrease the asymptotic estimation error. The  $\ell_2$ -norm was used so that the eigenvalues sum up to 1, but the results for  $\ell_1$ -norm are similar.

Even though we do not use information on the geographical locations, the first three eigenvectors shown in Figure 4 exhibit a clear spatial pattern. While the leading eigenvector points to the center of the simplex, the second eigenvector shows a linear trend from southeast to northwest. The third eigenvector exhibits a slightly more complicated spatial pattern. Figure 4 also shows a scree plot of the eigenvalues which quickly flattens. It is noted, however, that for  $p = 3$  the mean squared loss in Equation 19 evaluates to  $1 - \sum_{i=1}^3 \lambda_i = 0.57$ , which yields root mean squared error of about 0.75. The first three principal components thus explain 25% of the extremal dependence, while the first 20 explain about 65%.

## 5. Concomitant extremes

The identification of groups of variables that can be large simultaneously is one of the basic questions in multivariate extremes. Such groups  $I \subset V$  correspond to  $\chi_I > 0$ . The stronger condition  $\Lambda(\mathcal{E}_I) > 0$  asserts that the components indexed by  $I$  can be extreme

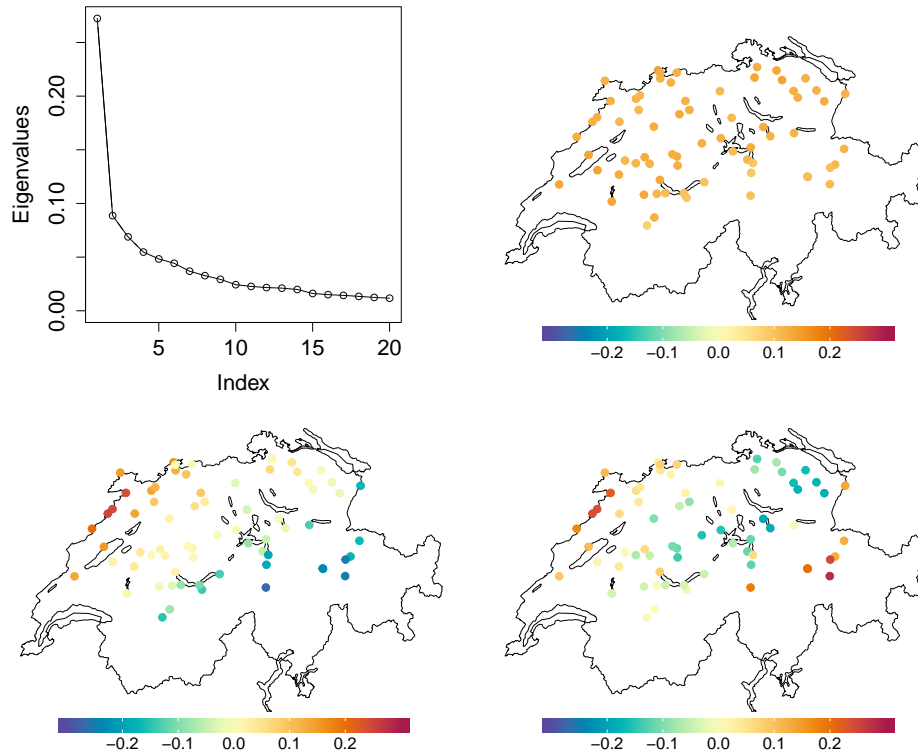


Figure 4: Scree plot of eigenvalues (top left) and the first three eigenvectors plotted at the corresponding geographical locations of the stations.

while the others are much smaller (cf., Section 2.4). In this respect, multivariate extremes are different from classical multivariate analysis where restriction of some variables to zero normally is of little interest.

**Example 4.** Figure 3 shows the extremal angles corresponding to the sub-group  $\{1, 56, 57\}$  of stations in the river application. In this case, visually, it seems that  $\Lambda$  puts mass on the faces  $\mathcal{E}_{\{1\}}$ ,  $\mathcal{E}_{\{2,3\}}$  and possibly  $\mathcal{E}_{\{1,2,3\}}$ . Note that station 1 is far apart from stations 56 and 57, whereas the latter two are close-by; see Figures 1 and 2. This means that floods can either occur at all stations simultaneously, possibly due to a large-scale precipitation event, or separately either at station 1 or at both stations 56 and 57 due to heavy localized rain.

In principle, it is possible that all combinations of extreme components may arise and  $\Lambda$  has mass on all  $2^d - 1$  faces. This situation, however, is rather unlikely in data applications, since we always expect some structure between the variables (cf., Example 4) and simply since the number of exceedances  $k(n)$  is usually much smaller than  $2^d - 1$ . Moreover, current statistical models are not flexible enough to jointly model complex dependence structures on all possible faces. They are mostly designed to separately model different subsets of variables which can be concomitantly extreme. If we knew the relevant faces and the

corresponding probabilities, a sensible modeling strategy would be to fit models on these faces separately and to combine them as a mixture model.

In order to make this feasible, one may assume a notion of sparsity in terms of the number and dimension of the faces of  $\mathcal{E}$  charged with mass (cf., Goix et al. 2017).

(S2.a) There is only a small number of groups of variables in  $(X_j : j \in V)$  that can be concomitantly extreme, that is,

$$|\{I \subset V : \Lambda(\mathcal{E}_I) > 0\}| \ll 2^d - 1.$$

(S2.b) Each of these groups contains only a small number of variables, that is,

$$\max\{|I| : \Lambda(\mathcal{E}_I) > 0\} \ll d.$$

The sparsity notion (S2.a) is the most crucial since it limits the number of components in a mixture model. If, in addition, the second notion (S2.b) holds, then each of the sub-models is low-dimensional and particularly simple. As we will see in Section 6, a different notion of sparsity for densities on the cones  $\mathcal{E}_I$  can be defined that allows to model simultaneous extremes for large  $|I|$ .

### 5.1. Detecting faces with $\Lambda$ -mass

Recall the set  $\mathcal{L}$  bounded away from the origin and consider its partition into

$$\mathcal{L}_I = \{x \in \mathcal{E}_I : \|x\|_\infty \geq 1\}.$$

We are interested in identifying subsets  $I$  such that  $\Lambda(\mathcal{L}_I) > 0$ , as well as the respective masses characterizing the weights in the mixture model. The main difficulty in estimation of these masses is that the convergence in Equation 7 does only hold for  $\Lambda$ -continuous sets, excluding sets  $\mathcal{L}_I$  charged with mass. We therefore cannot simply rely on empirical estimates of the left-hand side of Equation 7, because even for large  $t > 0$ , there will typically be no observation of  $X/t$  falling in  $\mathcal{L}_I$  since none of the components is exactly zero.

To circumvent this difficulty, Goix et al. (2016, 2017), propose to partition  $\mathcal{L}$  into sets

$$\mathcal{L}_I^\varepsilon = \{x \in \mathcal{L} : x_i > \varepsilon \forall i \in I, x_j \leq \varepsilon \forall j \notin I\} \quad 21.$$

for some small  $\varepsilon > 0$ , which they call  $\varepsilon$ -thickened rectangles; see the blue regions in Figure 5. In this setting Equation 7 is valid, and we can approximate  $\Lambda(\mathcal{L}_I)$  by  $t\mathbb{P}(X/t \in \mathcal{L}_I^\varepsilon)$  or rather its empirical estimate for some large threshold  $t$  (cf., Section 2.5). Since  $\Lambda(\mathcal{L}_I^\varepsilon)$  converges to  $\Lambda(\mathcal{L}_I)$  as  $\varepsilon \rightarrow 0$ , the authors argue that if  $\varepsilon$  is chosen small enough then essentially only mass that corresponds to the set  $\mathcal{L}_I$  will enter the estimate. If this empirical mass is larger than a threshold  $u$ , then the  $I$ th face is identified to have positive  $\Lambda$ -mass. Both thresholds  $\varepsilon$  and  $u$  are tuning parameters. One issue with this approach is that it may be that  $\Lambda(\mathcal{L}_I) = 0$  even though non-negligible mass  $\Lambda(\mathcal{L}_I^\varepsilon) > 0$  in the corresponding  $\varepsilon$ -thickened rectangle is detected. Too many groups of concomitant extremes may thus be identified, which is confirmed by simulation studies in Chiapino & Sabourin (2017) and Simpson et al. (2018). As discussed above, this is a serious issue countering the sparsity assumption (S2.a). A larger threshold  $u$  for the mass may not be an option since then too many exceedances are ignored.



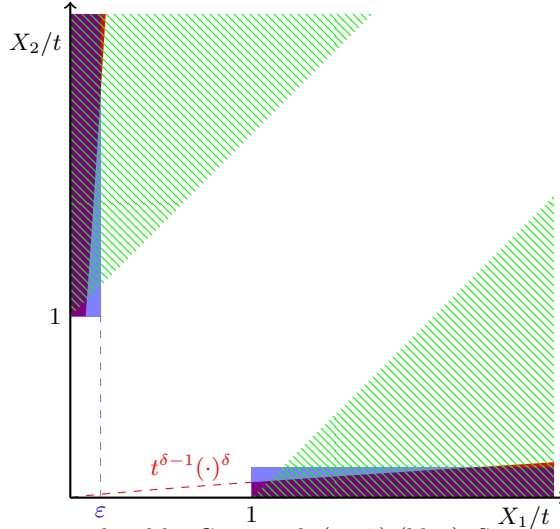


Figure 5: The regions considered by Goix et al. (2017) (blue), Simpson et al. (2018) (red) and Meyer & Wintenberger (2019) (green) to study the masses on faces  $\mathcal{E}_{\{1\}}$  (bottom right) and  $\mathcal{E}_{\{2\}}$  (top left) in the bivariate case.

In order to cope with this problem Simpson et al. (2018) suggest replacing the upper bound in the definition of  $\mathcal{L}_I^\varepsilon$  in Equation 21 by a more flexible threshold-dependent constraint  $\varepsilon_t$  with  $\varepsilon_t \rightarrow 0$  as  $t \rightarrow \infty$ . This still allows that  $\lim_{t \rightarrow \infty} t\mathbb{P}(X/t \in \mathcal{L}_I^{\varepsilon_t}) > 0$ . More precisely, their modeling strategy is to consider

$$\mathbb{P}\left(\min_{i \in I}(X_i/t) > 1, \max_{i \notin I}(X_i/t) \leq t^{\delta-1}\left(\min_{i \in I}(X_i/t)\right)^\delta\right), \quad 22.$$

for some  $\delta \in [0, 1)$ , and to assume that this probability is regularly varying as  $t \rightarrow \infty$ ; see the red regions in Figure 5. Note that if the probability in Equation 22 is of order  $1/t$  then  $\mathcal{E}_I$  must have a positive mass. For a fixed subset  $I$ , Simpson et al. (2018) use the Hill estimator (Hill 1975) to fit the model and then extrapolate this probability for large values of  $t$ . They propose to identify  $I$ th face to have positive  $\Lambda$ -mass if the corresponding approximation is larger than a suitable threshold  $u$ , similarly to Goix et al. (2017). Finally, the choice of  $\delta \in [0, 1)$  is a subtle trade-off between the significance level and the power of detecting mass on  $\mathcal{E}_I$ . If  $\delta$  is too close to one, then this procedure runs into the same issues as the method of Goix et al. (2017). On the other hand, if  $\delta$  is too small, then it can happen that no mass is detected even though  $\Lambda(\mathcal{E}_I) > 0$ .

**Remark 1.** *Importantly, the above procedures do not necessarily require processing all  $2^d - 1$  faces. Note that we can not identify more faces with mass than there are exceedances. Thus instead of cycling over the faces we can go over all exceedances, whose number is fairly small by definition.*

## 5.2. Detecting maximal faces with $\Lambda$ -mass

Recovering all faces  $\mathcal{E}_I$  with positive mass is a difficult problem. Moreover, it does not lead to a sparse representation when the mass is spread over a large number of faces. For the

data set on river discharges studied in Chiapino & Sabourin (2017), it was found that many of the detected groups of variables differ from each other only by a single or two elements. Practically speaking, this means that several distinct extreme events have impacted almost the same set of stations. This motivates gathering such groups into a single one and a natural approach is to look at maximal sets. More precisely, the aim is to identify groups  $I$  with  $\Lambda(\mathcal{E}_I) > 0$  such that  $\Lambda(\mathcal{E}_J) = 0$  for all  $J \supsetneq I$ . As noted by Chiapino & Sabourin (2017) this is the same as looking for the maximal sets with  $\chi_I > 0$ . Indeed, the latter implies that the variables indexed by  $I$  can be simultaneously extreme, and by maximality of  $I$  no further variables can be added.

Chiapino & Sabourin (2017) propose to use the Apriori algorithm (Agrawal et al. 1994) for frequent item set mining with a novel stopping criterion. This algorithm results in a bottom-up approach starting with singletons and at each step enlarging all the groups by one element if there is sufficient evidence that all the components can be concomitantly extreme. They use a threshold-based stopping criterion involving the empirical estimate of a conditional version of  $\chi_I$ . This conditional tail dependence coefficient is taken to avoid the problem that  $\chi_I$  decreases as the sets grow; see the comment following Equation 5. This work was extended by Chiapino et al. (2019) proposing three other stopping criteria based on formal hypothesis testing. In particular, they consider testing whether the residual tail dependence coefficient in Equation 4 satisfies  $\eta_I = 1$ , which, under a weak assumption, is equivalent to  $\chi_I > 0$ . They further derive asymptotic results for controlling the type-I error of this test, and show that it has a better performance in simulation studies. Such tests are applied to every sub-face of a maximal face with mass, which leads to multiple testing problems and potentially long running times. The Apriori algorithm is thus efficient only when (S2.b) holds true, whereas it has to pass through all  $2^d - 1$  subsets if  $\Lambda(\mathcal{E}_V) > 0$ .

Meyer & Wintenberger (2019) suggest another approach for recovering the maximal sets with mass. For all observations where  $\|X\|_1 > t$ , for a large  $t > 0$ , instead of the usual projection  $X/\|X\|_1$ , they use the Euclidean projection  $\pi_1(X/t)$  (cf., Duchi et al. 2008) onto the positive  $\ell_1$ -sphere  $\mathbb{S}_+^{d-1}$ . The projection  $\pi_1(x)$ ,  $x \in \mathbb{R}_+^d$ , is the point on  $\mathbb{S}_+^{d-1}$  that minimizes the  $\ell_2$ -distance to  $x$ . The limiting mass on the the  $I$ th face of the  $\ell_1$ -sphere is

$$m_I = \lim_{t \rightarrow \infty} \mathbb{P}(\pi_1(X/t) \in \mathcal{E}_I \mid \|X\|_1 > t), \quad 23.$$

see the green regions in Figure 5. The geometry of the Euclidean projection has the effect that possibly more mass is projected on sub-faces of  $\mathbb{S}_+^{d-1}$  than the spectral measure actually has (cf., Equation 10). Importantly, the maximal sets in  $\{I \subset V : m_I > 0\}$  coincide with the maximal sets having positive  $\Lambda$ -mass. Empirical estimates  $\hat{m}_I$  of  $m_I$  are used in Meyer & Wintenberger (2019) to find these maximal sets.

We conclude this section by noting that Lehtomaa & Resnick (2019) study a somewhat related problem of estimating the support of the extremal angle  $\Theta$ .

**Remark 2.** *The methods above for detecting maximal faces with  $\Lambda$ -mass have the clear limitation that if there is mass on a high-dimensional face, say  $\Lambda(\mathcal{E}_V) > 0$ , then no other face  $\mathcal{E}_I$  with  $I \subsetneq V$  can be detected, even if  $\Lambda(\mathcal{E}_I) > 0$ . These methods must therefore assume the sparsity notion (S2.b), since otherwise too much information is lost.*

### 5.3. Application to flood risk

We reconsider our flood risk application from Section 1.2 and aim to identify the groups of variables which can be concomitantly extreme. We do not attempt to fine-tune each of the

Table 1: The 10 different clusters with the dimensions of the associated faces and the number of exceedances.

Cluster #	1	2	3	4	5	6	7	8	9	10	Total
Dimension	15	10	13	10	19	8	17	15	8	14	129
No. of exceedances	12	21	21	9	28	10	26	28	14	33	202

methods, but rather to illustrate the main ideas.

As has already been observed in the literature (Chiapino & Sabourin 2017, Chiapino et al. 2019), the truncation method of Goix et al. (2017) yields a very large number of faces, most of which have a single associated extremal observation. The only faces with more observations are typically of dimension close to  $d$ .

We therefore follow the idea of Janssen & Wan (2019), explained in Section 4.1, and use clustering to find the prototypes of groups of concomitant extremes, to which we then apply thresholding as in Goix et al. (2017). Firstly, we obtain samples of the extremal angle  $\Theta$  for the  $\ell_1$ -norm (cf., Section 4.3) and then cluster them into  $p = 10$  groups using the angular dissimilarity in Equation 18. To each cluster center  $c_j \in \mathbb{S}_+^{d-1}$ ,  $j = 1, \dots, p$ , we associate the face  $I_j = \{i \in V : c_{ij} > 0.02\}$ , where the cutting point 0.02 is a tuning parameter regulating the number of components in each group. The resulting faces are all of moderate dimensions; see Table 1. Figure 6 shows the faces with more than 20 associated exceedances. The cluster #10 has the highest number of exceedances and the corresponding group  $I_{10} = \{2, 5, 9, 15, 16, 17, 18, 26, 34, 39, 46, 47, 56, 57\}$  (in magenta color) will be modeled after some minor changes in Section 6. Interestingly, the components of each face are grouped geographically even though no such information is used. We note that clustering with a slightly different number of clusters produces similar results. One can also increase the number of clusters, which eventually leads to associating each observed angle with a face (cf., Goix et al. 2017).

The bottom-up procedure of Chiapino & Sabourin (2017) runs into the problem that faces of a moderate dimension, say 20, require passing through more than  $10^6$  sub-groups. Nevertheless, their testing criteria can be used to adjust the above discovered faces. Instead of the bottom-up approach we can start with a face discovered by clustering and apply a greedy strategy to prune or expand this face. Such greedy pruning is applied to the face  $I_{10}$  and it suggests to exclude stations 2 and 34, since this results in a sharp increase of the associated tail dependence coefficient from 0.15 to 0.32.

## 6. Graphical models for extremes

Statistical modeling of a random vector  $X = (X_j : j \in V)$  with moderately large dimension  $|V| = d$  quickly becomes prohibitive because of the complexity of possible dependence structures between the variables. This is all the more true for extremes where current parametric models in higher dimension are either simplistic, e.g., the logistic model with just one parameter, or over-parameterized, e.g., the Hüsler-Reiss model with  $(d-1)d/2$  parameters; see Section 3. Apart from the number of parameters, statistical inference for extreme value models is challenging even in moderate dimensions.

Conditional independence and graphical models are classical tools for factorizations of high-dimensional densities, thereby leading to a number of low-dimensional models. Such simplified probabilistic structures facilitate inference and allow the construction of parsimonious

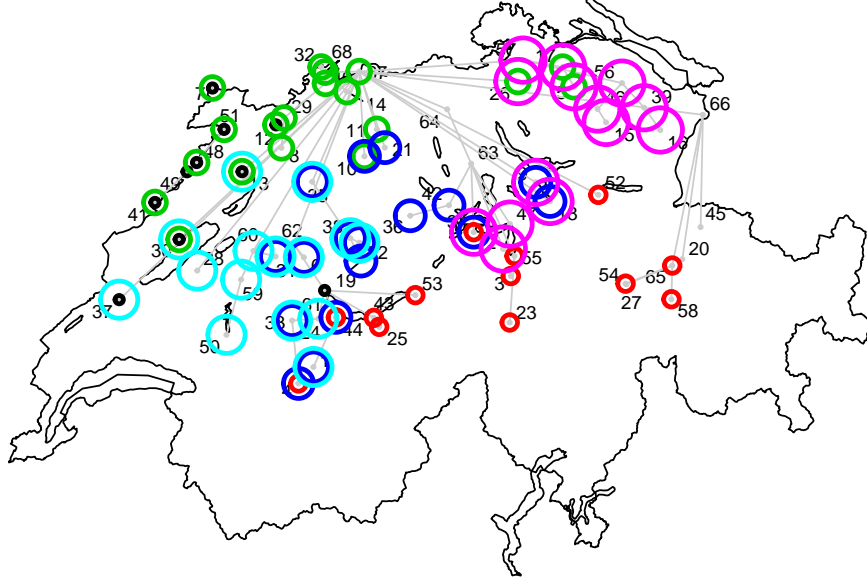


Figure 6: The 6 faces with more than 20 exceedances obtained by clustering angles into 10 groups and thresholding the centers at 0.02; the stations associated to each face have the same color and circle radius. The gray lines show the flow connections between the stations.

monious parametric models with possibly sparse patterns (Lauritzen 1996, Wainwright & Jordan 2008). A graphical model for the distribution of  $X$  is a set of conditional independence constraints that are encoded by a graph  $G = (V, E)$  with vertex set  $V$  and edge set  $E \subset V \times V$ . For disjoint subsets  $A, B, C \subset V$ , conditional independence between  $X_A$  and  $X_C$  given  $X_B$ , denoted by  $X_A \perp\!\!\!\perp X_C \mid X_B$ , is present if the paths between vertices in  $A$  and  $C$  are blocked by  $B$  in  $G$  in a suitable way; we refer to Lauritzen (1996, Chapter 2) and Drton & Maathuis (2017) for basic notions of directed and undirected graphs.

A sparse graph with few edges will induce many conditional independencies and the corresponding distribution can be explained by lower-dimensional objects. It is therefore natural to define sparsity in this framework in the following way.

- (S3) A graphical model is sparse if the number of edges is much smaller than the number of all possible edges, that is,

$$|E| \ll d^2. \quad 24.$$

In this section we review the recent literature that connect the two fields of extremes and graphical models.

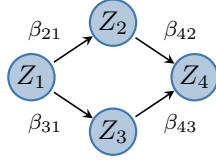


Figure 7: Directed acyclic graph  $G$  with  $d = 4$  vertices.

### 6.1. Max-stable distributions

Conditional independence is the basis for the factorization of multivariate densities. For a max-stable random vector  $Z = (Z_j : j \in V)$  Papastathopoulos & Strokorb (2016) showed a surprising negative result on the possibility of such factorizations. Suppose that  $Z$  possesses a positive continuous density and that for disjoint subsets  $A, B, C \subset V$ , the conditional independence

$$Z_A \perp\!\!\!\perp Z_C \mid Z_B,$$

holds. Then this already implies the unconditional independence  $Z_A \perp\!\!\!\perp Z_C$ . This means that no non-trivial conditional independencies are possible in this model class.

While the above result prevents the definition of sparse models for max-stable densities, it does not affect max-stable models that do not possess densities. An important class of such distributions are the max-linear models defined in Example 1. Gissibl & Klüppelberg (2018) introduce and study a particular sub-class of max-linear models that are defined on a directed acyclic graph (DAG). A DAG is a graph  $G = (V, E)$  with directed edges in  $E$  without directed cycles; see Figure 7 for an example in dimension  $d = 4$ . Following the approach of structural equation modeling (Spirtes et al. 2000, Pearl 2009), Gissibl & Klüppelberg (2018) define a recursive max-linear model on the DAG  $G$  by

$$Z_i = \bigvee_{j \in \text{pa}(i)} \beta_{ij} Z_j \vee \beta_{ii} \varepsilon_i, \quad i \in V, \quad 25.$$

where  $\beta_{ij} > 0$ ,  $\varepsilon_i$  are independent noise variables with standard Fréchet distribution and  $\text{pa}(i)$  denotes the graphical parents of the vertex  $i$ . It is readily verified that the model in Equation 25 can be written as a  $d$ -dimensional max-linear model with  $d$  factors defined in Equation 13 with coefficients  $a_{ij}$  that can be derived from the coefficients  $\beta_{ij}$ . This also implies that these models have discrete spectral measure with exactly  $d$  point masses.

With this construction, the  $d$ -dimensional max-stable random vector  $Z$  in Equation 25 does indeed satisfy certain conditional independence relations that are implied by the DAG through so-called  $d$ -separations. For instance, for the recursive max-linear model in Figure 7, we have that  $Z_1 \perp\!\!\!\perp Z_4 \mid \{Z_2, Z_3\}$  but  $\neg(Z_2 \perp\!\!\!\perp Z_3 \mid \{Z_1, Z_4\})$  (Klüppelberg & Lauritzen 2019).

For a fixed DAG, the estimation of the coefficients  $\beta_{ij}$  based on data from  $Z$  is challenging due to the discrete nature of max-linear distributions that prohibits standard maximum likelihood methods. Instead, Yuen & Stoev (2014), Einmahl et al. (2016) and Einmahl et al. (2018) use M-estimators to circumvent this issue, and Janssen & Wan (2019) apply the spherical  $k$ -means clustering described in Section 4.1 to do inference for max-linear models. Alternatively, Gissibl et al. (2019) use a generalized maximum likelihood estimator

(cf., Kiefer & Wolfowitz 1956). The authors of this work also propose a way of learning the graph structure from data. Further works in this field are Einmahl et al. (2018) who use recursive max-linear model to study European stock market, and Klüppelberg & Sönmez (2020) who extend recursive max-linear models to infinite graphs and study connections to percolation theory.

One interpretation of the recursive max-linear model on DAGs is in terms of Bayesian networks and causality. In this model, large errors propagate through the directed graph deterministically. In non-extreme statistics, linear structural equation models are common tools in causal inference. For standard Fréchet noise variables, similarly to Equation 25 we define

$$X_i = \sum_{j \in \text{pa}(i)} \beta_{ij} X_j + \beta_{ii} \varepsilon_i, \quad i \in V. \quad 26.$$

Despite their similar structure, the extremal behavior of the linear and max-linear structural equation models in Equations 26 and 25, respectively, may be different, as it is the case for the DAG in Figure 7 for instance. Such discrepancies disappear after these models are expanded into non-recursive forms. The causal structure of the model in Equation 26 has been studied in Gnecco et al. (2019) who propose a greedy search for learning its structure, and define a notion of causal effects in extremes.

The field of causality for extreme events has become a topic of high interest (e.g., Mhalla et al. 2019, Gnecco et al. 2019), in particular in connection with the attribution of weather extremes in climate science (eg., Hannart et al. 2016, Naveau et al. 2018, 2020).

## 6.2. Multivariate Pareto distributions

**6.2.1. Conditional independence and extremal graphical models.** The negative result by Papastathopoulos & Strokorb (2016) presented in Section 6.1 does not apply to multivariate Pareto distributions, which are the limits of threshold exceedances.

Recall from Section 2.3 the definition of a multivariate Pareto vector  $Y = (Y_j : j \in V)$  with support in  $\mathcal{L} = \{x \in \mathbb{R}_+^d : \|x\|_\infty \geq 1\}$ . Since this space is not a product space, the classical notions of independence and conditional independence are not applicable. Engelke & Hitz (2019) propose an alternative notion of extremal conditional independence for a multivariate Pareto distribution  $Y$ . For any  $m \in V$ , introduce the auxiliary random vector  $Y^m$  as  $Y$  conditioned on the event that  $\{Y_m > 1\}$ , which has support in the product space  $\{x \in \mathbb{R}_+^d : x_m \geq 1\}$ . For a partition  $\{A, B, C\}$  of  $V$ , we say that  $Y_A$  is conditionally independent of  $Y_C$  given  $Y_B$  if

$$\forall m \in \{1, \dots, d\} : \quad Y_A^m \perp\!\!\!\perp Y_C^m \mid Y_B^m. \quad 27.$$

In this case we write  $Y_A \perp_e Y_C \mid Y_B$ , where the subscript  $\perp_e$  indicates extremal independence. When the set  $B$  is empty it can be shown that  $Y_A \perp_e Y_C$  is equivalent to the classical definition of asymptotic extremal independence between  $Y_A$  and  $Y_C$  (Strokorb 2020) as defined in Section 2.2. The conditional independence notion  $\perp_e$  is therefore a natural extension to the case more complex conditional extremal independence structures.

From now on we consider undirected graphs  $G = (V, E)$ . An extremal graphical model is defined as a multivariate Pareto distribution  $Y$  that satisfies the pairwise Markov property on  $G$  with respect to the conditional independence relation  $\perp_e$ , that is,

$$Y_i \perp_e Y_j \mid Y_{V \setminus \{i, j\}} \quad \text{if } (i, j) \notin E. \quad 28.$$

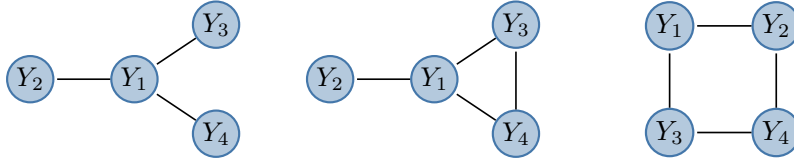


Figure 8: Three graphical models with  $d = 4$  vertices. The graphs on the left and in the center are decomposable, whereas the graph on the right is not decomposable.

Assume now that the graph  $G$  is decomposable; see Lauritzen (1996, Chapter 2) for the definition and Figure 8 for two examples of decomposable graphs. Then the analogue of the Hammersley–Clifford theorem holds for the extremal graphical model  $Y$  with a positive and continuous density  $f_Y$  on  $\mathcal{L}$ ; see Engelke & Hitz (2019). More precisely, the pairwise Markov property in Equation 28 on  $G$  is equivalent to the factorization

$$f_Y(y) = \frac{1}{\chi_V} \frac{\prod_{C \in \mathcal{C}} \lambda_C(y_C)}{\prod_{D \in \mathcal{D}} \lambda_D(y_D)}, \quad y \in \mathcal{L}, \quad 29.$$

where  $\mathcal{C}$  and  $\mathcal{D}$  are the sets of cliques and intersections between these cliques, respectively. The factors  $\lambda_I$  are the exponent measure densities corresponding to the vectors  $Y_I$  (cf., Section 2.3), and  $\chi_V$  is the tail dependence coefficient from Section 2.2. Moreover, in this case the graph  $G$  is necessarily connected, which means that all components are asymptotically dependent.

It is worthwhile to review some classical statistical models proposed in the literature regarding their sparsity properties. In fact, many existing models do not have any conditional independencies and their underlying graphs are fully connected. This holds for instance for the multivariate logistic distribution, the Dirichlet mixture model (Boldi & Davison 2007), and the pairwise beta distribution (Cooley et al. 2010). This observation explains why such models tend to be either too simple or over-parameterized in higher dimensions. For the simple example where the graph  $G$  is a chain, that is,

$$E = \{\{1, 2\}, \{2, 3\}, \dots, \{d-1, d\}\}, \quad 30.$$

Coles & Tawn (1991) propose a model that factorizes with respect to this graph where all bivariate marginals are logistic, and Smith et al. (1997) extend this to general bivariate marginals. More generally, this relates to the study of extremes of stationary Markov chains where the limiting objects are called tail chains. The multivariate Pareto distributions associated to tail chains factorize with respect to the chain graph; see Smith (1992), Basrak & Segers (2009) and Janssen & Segers (2014).

**6.2.2. Trees.** A tree  $T = (V, E)$  is a graph that is connected and has no cycles; see left-hand side of Figure 8 for an example. The number of edges in a tree equals to  $d - 1$ , all cliques consist of two vertices and the separator sets are singletons. A tree is thus the sparsest model among connected graphs in the sense of the sparsity notion (S3).

An extremal tree model is a multivariate Pareto distribution  $Y$  that satisfies the pairwise Markov property in Equation 28 on a tree  $T$ . Such models also appear as the limits of regular

varying Markov trees (Segers 2019). For extremal tree models, Equation 29 simplifies to

$$f_Y(y) = \frac{1}{\chi_V} \prod_{\{i,j\} \in E} \frac{\lambda_{ij}(y_i, y_j)}{y_i^{-2} y_j^{-2}} \prod_{i \in V} y_i^{-2}. \quad 31.$$

Apart from characterizing the density of extremal tree models, this formula also provides a way of constructing new models. If the tree structure is given or known, for instance through domain knowledge, Equation 31 can be used as a recipe to construct sparse, high-dimensional Pareto distributions from bivariate models. In fact, for any combination of the  $d - 1$  bivariate exponent measure densities  $(\lambda_{ij} : \{i, j\} \in E)$ , Equation 31 defines a valid  $d$ -dimensional Pareto distribution. Engelke & Hitz (2019) use the density of the bivariate Hüsler–Reiss distribution (cf., Example 3) with parameters  $\Gamma_{ij}$  for  $\lambda_{ij}$  and show that the resulting multivariate density  $f_Y$  is again a Hüsler–Reiss distribution with parameter matrix  $\Gamma = (\Gamma_{kl})_{k,l \in V}$  induced by the conditional independence structure, i.e.,

$$\Gamma_{kl} = \sum_{\{i,j\} \in \text{ph}(k,l)} \Gamma_{ij}, \quad k, l \in V, \quad 32.$$

where  $\text{ph}(k, l)$  denotes the set of edges on the unique path from vertex  $k$  to vertex  $l$  on the tree  $T$ . The number of free parameters in this model is thus  $d - 1$  and much smaller than the  $d(d - 1)/2$  parameters in the unrestricted parameter matrix  $\Gamma$ , thus satisfying the sparsity notion (S3) in Equation 24. This model was also used in Asenova et al. (2020) in the case where some vertices in the tree are unobserved.

For more flexible statistical modeling it is possible to use different parametric families for the  $\lambda_{ij}$ ,  $\{i, j\} \in E$ , or even model them with non-parametric methods. A natural extension of trees are so-called block graphs, i.e., decomposable graphs with singleton separator sets; see, for instance, the graphs on the left-hand side and in the center of Figure 8. For this class of graphical structures, similar formulas as in Equations 31 and 32 hold and the same modular modeling strategy can be used (cf., Engelke & Hitz 2019, Section 5).

In most applications, the underlying tree structure is not known and domain knowledge may be unavailable or insufficient. In such cases, the conditional independence structure must be learned from data. A common tool to this end is the notion of a minimum spanning tree. For each possible edge  $\{i, j\}$  between two vertices  $i, j \in V$ , let  $w_{ij} > 0$  be a weight, which can be seen as the length of this edge. It is assumed that  $w_{ij} = w_{ji}$  and  $w_{ii} = 0$ ,  $i, j \in V$ . The minimum spanning tree is the tree that minimizes the sum of its edge weights

$$T_{\text{mst}} = \arg \min_{T=(V,E)} \sum_{\{i,j\} \in E} w_{ij}. \quad 33.$$

The set of all possible trees is very large, but there exist efficient greedy algorithms to solve this problem even for large dimensions  $d$  (Kruskal 1956, Prim 1957). The main difficulty is the suitable choice of weights that guarantees that the minimum spanning tree  $T_{\text{mst}}$  coincides with the underlying conditional independence tree  $T$ .

In the non-extremal case of multivariate Gaussian distributions with correlation matrix  $(\rho_{ij})_{i,j \in V}$ , it can be shown that choosing  $w_{ij} = -\log |\rho_{ij}|$  (or any monotonically increasing transformation of it) yields the true Gaussian tree structure as the minimum spanning tree (cf., Drton & Maathuis 2017). The assumption of Gaussianity is crucial and the result no longer holds outside of this specific parametric class.

For a multivariate Pareto distribution  $Y$  factorizing on a tree  $T$ , Engelke & Volgushev (2020) show that the bivariate extremal correlation coefficients introduced in Equation 3



can be used for structure learning. In fact, letting

$$w_{ij} = -\log \chi_{ij}, \quad i, j \in V, \quad 34.$$

the minimum spanning tree in Equation 33 satisfies  $T_{\text{mst}} = T$ . It should be noted that this result holds regardless of the distribution of  $Y$  and no assumption on a specific parametric model class is required. This is quite surprising, since it is stronger than in the classical, non-extremal theory of trees. Engelke & Volgushev (2020) further introduce a new summary statistic, the extremal variogram, which can also be used in Equation 33 to consistently recover the extremal tree structure, and which tends to be more accurate in finite samples. An alternative approach is to use likelihood based methods to learn the tree structure. This requires to specify a parametric model class, but it also allows to learn certain block graph structures by a forward selection algorithm (cf., Engelke & Hitz 2019).

**6.2.3. Hüsler–Reiss graphical models.** Going beyond trees and block graphs requires a distributional assumption on the multivariate Pareto distribution. The Hüsler–Reiss distribution, introduced in Example 3, can be seen as the natural analogue of Gaussian distributions in the world of asymptotically dependent extremes.

While for a multivariate Gaussian distribution with covariance matrix  $\Sigma$  the conditional independence structure can be identified from the zeros on the precision matrix  $\Sigma^{-1}$ , for Hüsler–Reiss distributions the conditionally negative definite parameter matrix  $\Gamma$  plays the key role. Recall from Equation 16 the matrix  $\Sigma^{(m)}$ , which is of dimension  $(d-1) \times (d-1)$  since the  $m$ th row and column are omitted. Engelke & Hitz (2019, Proposition 3) show that for any  $m \in V$ , the inverse  $K^{(m)}$  of the matrix  $\Sigma^{(m)}$  satisfies

$$Y_i \perp_e Y_j \mid Y_{V \setminus \{i,j\}} \iff \begin{cases} K_{ij}^{(m)} = 0, & \text{if } i, j \neq m, \\ \sum_{l \neq m} K_{il}^{(m)} = 0, & \text{if } i \neq m, j = m. \end{cases} \quad 35.$$

For any  $m \in V$ , the single matrix  $K^{(m)}$  contains all information on the extremal graphical structure. Edges between vertices not including the  $m$ th vertex correspond to zeros on the off-diagonal, while edges including the  $m$ th vertex correspond to zero row sums. This result holds for any graph, even if it is not decomposable.

Hüsler–Reiss distributions are the finite dimensional distributions of Brown–Resnick processes, a widely used model for spatial extreme events parameterized by variogram functions (Brown & Resnick 1977, Kabluchko et al. 2009). Equation 35 can be used to see that most popular parametric classes of variogram functions yield models that do not have any conditional independencies. An exception is the original Brown–Resnick process introduced in Brown & Resnick (1977) whose finite dimensional distributions factorize on the chain graph in Equation 30.

### 6.3. Application to flood risk

In Section 5.3 the group of stations  $I_{10}$  was identified as the one manifesting most frequent concomitant extremes; it was then adjusted by removing stations 2 and 34. For illustration purposes, we add the larger downstream stations 63, 64 and 67, and then analyze this group of 15 stations with the extremal graphical models in Section 6.2. We use the R (R Core Team 2019) implementation of the package `graphicalExtremes` (Engelke et al. 2019b) for structure learning and model fitting.

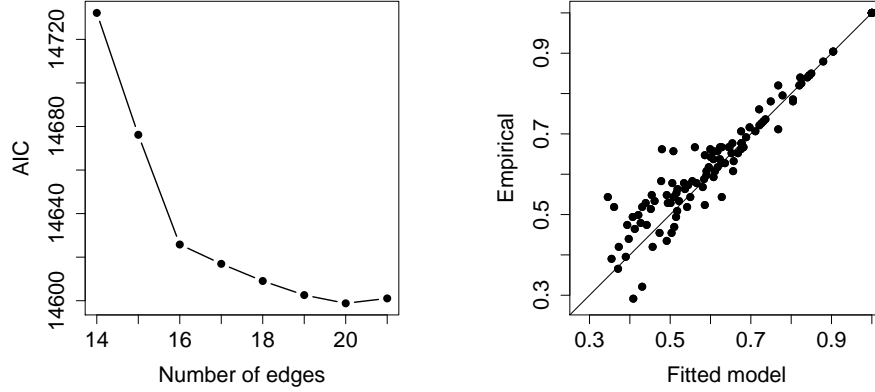


Figure 9: Left: AIC values for extremal graphical models for the river data set with an increasing number of edges, starting from the minimum spanning tree. Right: empirically estimated  $\hat{\chi}_{ij}$  coefficients for all pairs of stations against those implied by the fitted graphical model minimizing the AIC.

We do not use any geographical information on the locations but learn the graph structure from the data. First, we estimate the minimum spanning tree  $T_{\text{mst}}$  with weights  $-\log \hat{\chi}_{ij}$  based on the empirical tail dependence coefficients; see Section 6.2.2. We choose to use a Hüsler–Reiss distribution on the tree structure, and then extend this model by adding edges in a greedy way while staying in the class of block graphs with cliques of maximal size three (cf., Engelke & Hitz 2019, Section 6). Fitting these models requires maximization of bivariate and trivariate Hüsler–Reiss densities with censoring for non-extreme components (cf., Ledford & Tawn 1997). The greedy forward selection is based on the AIC score.

The AIC curve of the resulting model fits is shown on the left-hand side of Figure 9. The best model minimizing the AIC has 20 edges and is significantly better than the simpler tree model. Note that the number of 20 free parameters in this block graph model is much lower than the 105 parameters in a dense Hüsler–Reiss model with  $d = 15$ . Moreover, because of the density decomposition in Equation 29, the parameters on each of the cliques can be estimated separately, rendering inference much more efficient (cf., Engelke & Hitz 2019, Section 5). The estimated graph structure of the best model is shown in Figure 10. We note that the graph does only roughly reflect the flow connections in the river network in Figure 1. This is not a contradiction, since other effects such as spatial precipitation events may affect dependence between the peak flows. For instance, the fact that the stations 63 and 64 are not directly connected to station 47 may be due to the large lakes that dampen the largest discharges. The right-hand side of Figure 9 compares empirical estimates  $\hat{\chi}_{ij}$  of the tail dependence coefficients between all 15 stations with those implied by the best fitted model. The plot underlines that the sparse graphical Hüsler–Reiss model captures well the extremal dependence in the data.

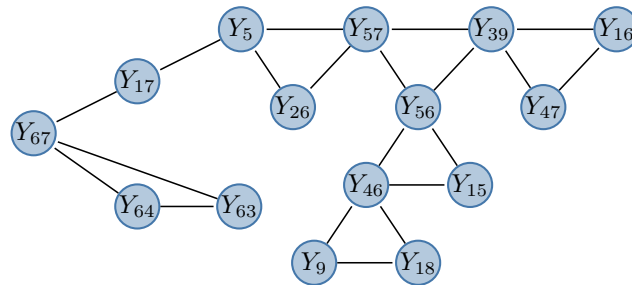


Figure 10: The estimated block graph corresponding to the model with the optimal AIC.

### FUTURE ISSUES

1. Adaptation of further methods from multivariate analysis and machine learning for rare event modeling.
2. Automatic and efficient search algorithms to select out of all  $2^d - 1$  possible faces those with  $\Lambda$  mass.
3. Structure estimation methods for extremal graphical models beyond trees and automatic selection of the degree of sparsity.
4. Modeling sparse structures in sub-asymptotic extremes for asymptotically independent data.
5. Flexible sparse models for mixtures of asymptotic independence and dependence.
6. Modeling and detection of causal effects in the distributional tails.
7. Methods for extreme value analysis in high-dimensional settings  $d \gg n$ .

### ACKNOWLEDGMENTS

J. Ivanovs gratefully acknowledges financial support of Sapere Aude Starting Grant 8049-00021B “Distributional Robustness in Assessment of Extreme Risk”.

### References

- Aas K, Czado C, Frigessi A, Bakken H. 2009. Pair-copula constructions of multiple dependence. *Insurance: Mathematics and Economics* 44:182 – 198
- Agrawal R, Srikant R, et al. 1994. Fast algorithms for mining association rules, In *Proceedings of the 20th International Conference on Very Large Data Bases, VLDB*, vol. 1215, pp. 487–499
- Anderson TW. 2003. An introduction to multivariate statistical analysis. Wiley Series in Probability and Statistics. Wiley-Interscience [John Wiley & Sons], Hoboken, NJ, 3rd ed.
- Asadi P, Davison AC, Engelke S. 2015. Extremes on river networks. *The Annals of Applied Statistics* 9:2023–2050
- Asadi P, Engelke S, Davison A. 2018. Optimal regionalization of extreme value distributions for flood estimation. *Journal of Hydrology* 556:182–193
- Asenova S, Mazo G, Segers J. 2020. Inference on extremal dependence in a latent markov tree model attracted to a Hüsler–Reiss distribution. Available from <https://arxiv.org/abs/2001.09510>

- Balkema AA, de Haan L. 1974. Residual life time at great age. *Ann. Probability* 2:792–804
- Basrak B, Davis RA, Mikosch T. 2002. A characterization of multivariate regular variation. *The Annals of Applied Probability* 12:908–920
- Basrak B, Segers J. 2009. Regularly varying multivariate time series. *Stochastic Processes and their Applications* 119:1055 – 1080
- Beirlant J, Goegebeur Y, Teugels J, Segers J. 2004. Statistics of Extremes. Wiley Series in Probability and Statistics. John Wiley & Sons, Ltd., Chichester
- Bernard E, Naveau P, Vrac M, Mestre O. 2013. Clustering of maxima: Spatial dependencies among heavy rainfall in france. *Journal of Climate* 26:7929–7937
- Blanchard G, Bousquet O, Zwald L. 2007. Statistical properties of kernel principal component analysis. *Machine Learning* 66:259–294
- Boldi MO, Davison AC. 2007. A mixture model for multivariate extremes. *Journal of the Royal Statistical Society. Series B. Statistical Methodology* 69:217–229
- Brown BM, Resnick SI. 1977. Extreme values of independent stochastic processes. *J. Appl. Probab.* 14:732–739
- Bücher A, Segers J, Volgushev S. 2014. When Uniform Weak Convergence Fails: Empirical Processes for Dependence Functions and Residuals via Epi- and Hypographs. *Ann. Stat.* 42:1598–1634
- Chautru E. 2015. Dimension reduction in multivariate extreme value analysis. *Electron. J. Statist.* 9:383–418
- Chiapino M, Sabourin A. 2017. Feature clustering for extreme events analysis, with application to extreme stream-flow data, In *New Frontiers in Mining Complex Patterns*, eds. A Appice, M Ceci, C Loglisci, E Masciari, ZW Raś, pp. 132–147, Cham: Springer International Publishing
- Chiapino M, Sabourin A, Segers J. 2019. Identifying groups of variables with the potential of being large simultaneously. *Extremes* 22:193–222
- Coles S, Heffernan J, Tawn J. 1999. Dependence measures for extreme value analyses. *Extremes* 2:339–365
- Coles SG. 2001. An introduction to statistical modeling of extreme values. Springer Series in Statistics. Springer
- Coles SG, Tawn JA. 1991. Modelling extreme multivariate events. *Journal of the Royal Statistical Society. Series B. Methodological* 53:377–392
- Cooley D, Davis RA, Naveau P. 2010. The pairwise beta distribution: A flexible parametric multivariate model for extremes. *Journal of Multivariate Analysis* 101:2103–2117
- Cooley D, Thibaud E. 2019. Decompositions of dependence for high-dimensional extremes. *Biometrika* 106:587–604
- Davis RA, Klüppelberg C, Steinkohl C. 2013. Statistical inference for max-stable processes in space and time. *J. R. Stat. Soc. Ser. B Stat. Methodol.* 75:791–819
- Davison A, Huser R. 2015. Statistics of extremes. *Annual Review of Statistics and Its Application* 2:203–235
- Davison AC, Padoan SA, Ribatet M. 2012. Statistical modeling of spatial extremes. *Statist. Sci.* 27:161–186
- de Fondeville R, Davison AC. 2018. High-dimensional peaks-over-threshold inference. *Biometrika* 105:575–592
- de Haan L, Ferreira A. 2006. Extreme value theory. New York: Springer
- de Haan L, Zhou C. 2011. Extreme residual dependence for random vectors and processes. *Adv. in Appl. Probab.* 43:217–242
- Dhillon IS, Modha DS. 2001. Concept decompositions for large sparse text data using clustering. *Machine learning* 42:143–175
- Dieker AB, Mikosch T. 2015. Exact simulation of Brown–Resnick random fields at a finite number of locations. *Extremes* 18:301–314
- Dombry C, Engelke S, Oesting M. 2016. Exact simulation of max-stable processes. *Biometrika* 103:303–317

- Dombry C, Engelke S, Oesting M. 2017a. Asymptotic properties of the maximum likelihood estimator for multivariate extreme value distributions. Available from <https://arxiv.org/abs/1612.05178>
- Dombry C, Engelke S, Oesting M. 2017b. Bayesian inference for multivariate extreme value distributions. *Electronic Journal of Statistics* 11:4813–4844
- Dombry C, Eyi-Minko F, Ribatet M. 2013. Conditional simulation of max-stable processes. *Biometrika* 100:111–124
- Drees H, Huang X. 1998. Best attainable rates of convergence for estimators of the stable tail dependence function. *Journal of Multivariate Analysis* 64:25–46
- Drees H, Sabourin A. 2019. Principal component analysis for multivariate extremes. Available from <https://arxiv.org/abs/1906.11043>.
- Drton M, Maathuis MH. 2017. Structure learning in graphical modeling. *Annual Review of Statistics and Its Application* 4:365–393
- Duchi J, Shalev-Shwartz S, Singer Y, Chandra T. 2008. Efficient projections onto the  $l_1$ -ball for learning in high dimensions, In *Proceedings of the 25th international conference on Machine learning*, pp. 272–279, ACM
- Eastoe EF, Tawn JA. 2012. Modelling the distribution of the cluster maxima of exceedances of subasymptotic thresholds. *Biometrika* 99:43–55
- Einmahl J, Krajina A, Segers J. 2012a. An M-Estimator for Tail Dependence in Arbitrary Dimensions. *Ann. Stat.* 40:1764–1793
- Einmahl JHJ, Kiriliouk A, Krajina A, Segers J. 2016. An M-estimator of spatial tail dependence. *J. R. Stat. Soc. Ser. B. Stat. Methodol.* 78:275–298
- Einmahl JHJ, Kiriliouk A, Segers J. 2018. A continuous updating weighted least squares estimator of tail dependence in high dimensions. *Extremes* 21:205–233
- Einmahl JHJ, Krajina A, Segers J. 2012b. An M-estimator for tail dependence in arbitrary dimensions. *Ann. Statist.* 40:1764–1793
- Embrechts P, Klüppelberg C, Mikosch T. 1997. Modelling extremal events: for insurance and finance. London: Springer
- Engelke S, de Fondeville R, Oesting M. 2019a. Extremal behaviour of aggregated data with an application to downscaling. *Biometrika* 106:127–144
- Engelke S, Hitz A. 2019. Graphical models for extremes (with discussion). *Accepted in J. R. Stat. Soc. Ser. B Stat. Methodol.* Available from <https://arxiv.org/abs/1812.01734>.
- Engelke S, Hitz SA, Gnecco N. 2019b. graphicalExtremes: Statistical methodology for graphical extreme value models. Available from <https://CRAN.R-project.org/package=graphicalExtremes>, R package version 0.1.0
- Engelke S, Malinowski A, Kabluchko Z, Schlather M. 2015. Estimation of Hüsler–Reiss distributions and Brown–Resnick processes. *Journal of the Royal Statistical Society. Series B. Methodological* 77:239–265
- Engelke S, Opitz T, Wadsworth J. 2019c. Extremal dependence of random scale constructions. *Extremes* 22:623–666
- Engelke S, Volgushev S. 2020. The extremal variogram and tree structure learning. In preparation
- Fisher RA, Tippett LHC. 1928. Limiting forms of the frequency distribution of the largest or smallest member of a sample, In *Mathematical Proceedings of the Cambridge Philosophical Society*, vol. 24, pp. 180–190, Cambridge University Press
- Gissibl N, Klüppelberg C. 2018. Max-linear models on directed acyclic graphs. *Bernoulli* 24:2693–2720
- Gissibl N, Klüppelberg C, Lauritzen S. 2019. Identifiability and estimation of recursive max-linear models. *arXiv preprint arXiv:1901.03556*
- Gnecco N, Meinshausen N, Peters J, Engelke S. 2019. Causal discovery in heavy-tailed models. Available from <https://arxiv.org/abs/1908.05097>.
- Goix N, Sabourin A, Clmenon S. 2016. Sparse representation of multivariate extremes with appli-

- cations to anomaly ranking, In *Proceedings of the 19th International Conference on Artificial Intelligence and Statistics (AISTATS)*. JMLR: W&CP
- Goix N, Sabourin A, Clmenon S. 2017. Sparse representation of multivariate extremes with applications to anomaly detection. *Journal of Multivariate Analysis* 161:12 – 31
- Gudendorf G, Segers J. 2010. Extreme-value copulas. In *Copula Theory and Its Applications*. Springer, 127–145
- Hannart A, Pearl J, Otto FEL, Naveau P, Ghil M. 2016. Causal counterfactual theory for the attribution of weather and climate-related events. *Bulletin of the American Meteorological Society* 97:99–110
- Haug S, Klüppelberg C, Kuhn G. 2009. Dimension reduction based on extreme dependence
- Heffernan JE, Tawn JA. 2004. A conditional approach for multivariate extreme values (with discussion). *Journal of the Royal Statistical Society: Series B (Statistical Methodology)* 66:497–546
- Hill BM. 1975. A simple general approach to inference about the tail of a distribution. *Ann. Statist.* 3:1163–1174
- Hitz SA, Evans JR. 2016. One-component regular variation and graphical modeling of extremes. *Journal of Applied Probability* 53:733–746
- Huang X. 1992. Statistics of bivariate extreme value theory. Ph.D. thesis, Erasmus University Rotterdam
- Huser R, Dombry C, Ribatet M, Genton MG. 2019. Full likelihood inference for max-stable data. *Stat* 8:e218
- Huser R, Wadsworth JL. 2019. Modeling spatial processes with unknown extremal dependence class. *J. Amer. Statist. Assoc.* 114:434–444
- Hüsler J, Reiss RD. 1989. Maxima of normal random vectors: between independence and complete dependence. *Statistics & Probability Letters* 7:283–286
- Janssen A, Segers J. 2014. Markov tail chains. *Journal of Applied Probability* 51:1133–1153
- Janssen A, Wan P. 2019.  $k$ -means clustering of extremes. Available from <https://arxiv.org/abs/1904.02970>.
- Jung S, Dryden IL, Marron JS. 2012. Analysis of principal nested spheres. *Biometrika* 99:551–568
- Kabluchko Z, Schlather M, de Haan L. 2009. Stationary max-stable fields associated to negative definite functions. *Ann. Probab.* 37:2042–2065
- Katz RW, Parlange MB, Naveau P. 2002. Statistics of extremes in hydrology. *Advances in Water Resources* 25:1287–1304
- Keef C, Tawn J, Svensson C. 2009. Spatial risk assessment for extreme river flows. *J. R. Stat. Soc. Ser. C. Appl. Stat.* 58:601–618
- Kiefer J, Wolfowitz J. 1956. Consistency of the maximum likelihood estimator in the presence of infinitely many incidental parameters. *Ann. Math. Statist.* 27:887–906
- Klüppelberg C, Lauritzen S. 2019. Bayesian networks for max-linear models. Available from <https://arxiv.org/abs/1901.03948>.
- Klüppelberg C, Sönmez E. 2020. Max-linear models on infinite graphs generated by bernoulli bond percolation. Available from <https://arxiv.org/abs/1804.06102>
- Kruskal Jr. JB. 1956. On the shortest spanning subtree of a graph and the traveling salesman problem. *Proceedings of the American Mathematical Society* 7:48–50
- Larsson M, Resnick SI. 2012. Extremal dependence measure and extremogram: the regularly varying case. *Extremes* 15:231–256
- Lauritzen SL. 1996. Graphical models. Oxford University Press
- Ledford AW, Tawn JA. 1997. Modelling dependence within joint tail regions. *Journal of the Royal Statistical Society: Series B (Statistical Methodology)* 59:475–499
- Lee D, Joe H. 2018. Multivariate extreme value copulas with factor and tree dependence structures. *Extremes* 21:147–176
- Lehtomaa J, Resnick S. 2019. Asymptotic independence and support detection techniques for heavy-tailed multivariate data. *arXiv preprint arXiv:1904.00917*

- Lindskog F, Resnick SI, Roy J. 2014. Regularly varying measures on metric spaces: hidden regular variation and hidden jumps. *Probab. Surv.* 11:270–314
- McNeil AJ, Frey R, Embrechts P. 2015. Quantitative risk management: Concepts, techniques and tools. Princeton University Press
- Meyer N, Wintenberger O. 2019. Sparse regular variation. Available from <https://arxiv.org/abs/1907.00686>.
- Mhalla L, Chavez-Demoulin V, Dupuis DJ. 2019. Causal mechanism of extreme river discharges in the upper danube basin network. Available from <https://arxiv.org/abs/1907.03555>.
- Naveau P, Hannart A, Ribes A. 2020. Statistical methods for extreme event attribution in climate science. *Annual Review of Statistics and Its Application* To appear
- Naveau P, Ribes A, Zwiers F, Hannart A, Tuel A, Yiou P. 2018. Revising return periods for record events in a climate event attribution context. *Journal of Climate* 31:3411–3422
- Opitz T. 2013. Extremal  $t$  processes: Elliptical domain of attraction and a spectral representation. *J. Multivariate Anal.* 122:409–413
- Padoan SA, Ribatet M, Sisson SA. 2010. Likelihood-based inference for max-stable processes. *J. Amer. Statist. Assoc.* 105:263–277
- Papastathopoulos I, Strokorb K. 2016. Conditional independence among max-stable laws. *Statistics & Probability Letters* 108:9–15
- Papastathopoulos I, Strokorb K, Tawn JA, Butler A. 2017. Extreme events of Markov chains. *Advances in Applied Probability* 49:134–161
- Pearl J. 2009. Causality. Cambridge University Press, Cambridge, 2nd ed. Models, reasoning, and inference
- Peng L. 1999. Estimation of the coefficient of tail dependence in bivariate extremes. *Statist. Probab. Lett.* 43:399–409
- Pickands III J. 1975. Statistical inference using extreme order statistics. *The Annals of Statistics* 3:119–131
- Poon SH, Rockinger M, Tawn J. 2004. Extreme value dependence in financial markets: Diagnostics, models, and financial implications. *Rev. Financ. Stud.* 17:581–610
- Prim RC. 1957. Shortest connection networks and some generalizations. *Bell System Technical Journal* 36:1389–1401
- R Core Team. 2019. R: A language and environment for statistical computing. R Foundation for Statistical Computing, Vienna, Austria
- Ramos A, Ledford A. 2009. A new class of models for bivariate joint tails. *J. R. Stat. Soc. Ser. B Stat. Methodol.* 71:219–241
- Reich BJ, Shaby BA. 2012. A hierarchical max-stable spatial model for extreme precipitation. *Ann. Appl. Stat.* 6:1430–1451
- Resnick SI. 2008. Extreme values, regular variation and point processes. New York: Springer
- Rootzén H, Tajvidi N. 2006. Multivariate generalized Pareto distributions. *Bernoulli* 12:917–930
- Samorodnitsky G, Resnick S, Towsley D, Davis R, Willis A, Wan P. 2016. Nonstandard regular variation of in-degree and out-degree in the preferential attachment model. *Journal of Applied Probability* 53:146161
- Saunders KR, Stephenson AG, Karoly DJ. 2019. A regionalisation approach for rainfall based on extremal dependence. Available from <https://arxiv.org/abs/1907.05750>.
- Schlather M. 2002. Models for stationary max-stable random fields. *Extremes* 5:33–44
- Schlather M, Tawn J. 2002. Inequalities for the extremal coefficients of multivariate extreme value distributions. *Extremes* 5:87–102
- Seber GAF. 1984. Multivariate observations. Wiley Series in Probability and Mathematical Statistics: Probability and Mathematical Statistics. John Wiley & Sons, Inc., New York
- Segers J. 2019. One- versus multi-component regular variation and extremes of Markov trees. Available from <https://arxiv.org/abs/1902.02226>.
- Simpson E, Wadsworth J, Tawn J. 2018. Determining the dependence structure of multivariate

- extremessparse regular variation. Available from <https://arxiv.org/abs/1809.01606>.
- Smith R, Tawn J, Coles S. 1997. Markov chain models for threshold exceedances. *Biometrika* 84:249–268
- Smith RL. 1992. The extremal index for a markov chain. *Journal of Applied Probability* 29:3745
- Spirtes P, Glymour C, Scheines R. 2000. Causation, prediction, and search. MIT Press, Cambridge, MA, 2nd ed.
- Strokorb K. 2020. Extremal independence old and new. Available from <https://arxiv.org/abs/2002.07808>.
- Strokorb K, Schlather M. 2015. An exceptional max-stable process fully parameterized by its extremal coefficients. *Bernoulli* 21:276–302
- Tawn JA. 1988. Bivariate extreme value theory: Models and estimation. *Biometrika* 75:397–415
- Thibaud E, Aalto J, Cooley DS, Davison AC, Heikkinen J. 2016. Bayesian inference for the Brown–Resnick process, with an application to extreme low temperatures. *Ann. Appl. Stat.* 10:2303–2324
- Varin C, Reid N, Firth D. 2011. An overview of composite likelihood methods. *Statistica Sinica* 21:5–42
- Wackernagel H. 2013. Multivariate geostatistics. Springer, New York. An introduction with applications
- Wadsworth JL, Tawn JA. 2012. Dependence modelling for spatial extremes. *Biometrika* :asr080
- Wadsworth JL, Tawn JA. 2014. Efficient inference for spatial extreme value processes associated to log-Gaussian random functions. *Biometrika* 101:1–15
- Wadsworth JL, Tawn JA, Davison AC, Elton DM. 2017. Modelling across extremal dependence classes. *Journal of the Royal Statistical Society: Series B (Statistical Methodology)* 79:149–175
- Wainwright MJ, Jordan MI. 2008. Graphical models, exponential families, and variational inference. *Foundations and Trends in Machine Learning* 1:1–305
- Wan P, Wang T, Davis RA, Resnick SI. 2020. Are extreme value estimation methods useful for network data? *Extremes* 23:171–195
- Westra S, Sisson SA. 2011. Detection of non-stationarity in precipitation extremes using a max-stable process model. *Journal of Hydrology* 406:119 – 128
- Yu H, Uy WIT, Dauwels J. 2017. Modeling spatial extremes via ensemble-of-trees of pairwise copulas. *IEEE Transactions on Signal Processing* 65:571–586
- Yuen R, Stoev S. 2014. CRPS M-estimation for max-stable models. *Extremes* 17:387–410
- Zhou C. 2010. Dependence structure of risk factors and diversification effects. *Insur. Math. Econ.* 46:531–540
- Zou N, Volgushev S, Bücher A. 2019. Multiple block sizes and overlapping blocks for multivariate time series extremes. *arXiv preprint arXiv:1907.09477*
- Zscheischler J, Seneviratne SI. 2017. Dependence of drivers affects risks associated with compound events. *Science Advances* 3